

Predicting gene essentiality and drug response from perturbation screens in preclinical cancer models with LEAP: Layered Ensemble of Autoencoders and Predictors

Authors Barbara Bodinier*, Gaetan Dissez*, Linus Bleinstein, Antonin Dauvin#

* These authors contributed equally

Corresponding author

Abstract

Preclinical perturbation screens, where the effects of genetic, chemical, or environmental perturbations are systematically tested on disease models, hold significant promise for machine learning-enhanced drug discovery due to their scale and causal nature. Predictive models can infer perturbation responses for previously untested disease models based on molecular profiles. These *in silico* labels can expand databases and guide experimental prioritization. However, modelling perturbation-specific effects and generating robust prediction performances across diverse biological contexts remain elusive.

We introduce LEAP (Layered Ensemble of Autoencoders and Predictors), a novel ensemble framework to improve robustness and generalization. LEAP leverages multiple DAMAE (Data Augmented Masked Autoencoder) representations and LASSO regressors. By combining diverse gene expression representation models learned from different random initializations, LEAP consistently outperforms state-of-the-art approaches in predicting gene essentiality or drug responses in unseen cell lines, tissues and disease models. Notably, our results show that ensembling representation models, rather than prediction models alone, yields superior predictive performance.

Beyond its performance gains, LEAP is computationally efficient, requires minimal hyperparameter tuning and can therefore be readily incorporated into drug discovery pipelines to prioritize promising targets and support biomarker-driven stratification. The code and datasets used in this work are made publicly available.

Introduction

Preclinical experiments are essential in drug discovery. They are used to assess the properties and mechanisms of novel therapeutic targets and compounds in disease models, helping to validate efficacy, mitigate risks and address safety concerns before advancing to clinical trials. Amongst them, gene and drug perturbation screens have transformed preclinical studies by enabling the systematic evaluation of a vast number of perturbations across diverse biological contexts, helping the identification and positioning of novel therapeutic targets and compounds¹⁻⁴. These datasets are particularly valuable because the perturbations—whether genetic knockouts or compound treatments—are applied in a controlled experimental setting, allowing for direct observation of cause-and-effect relationships.

In oncology, significant initiatives have been undertaken to create and publicly share datasets of unprecedented scale. The Cancer Dependency Map (DepMap) project⁵, for instance, contains data on the essentiality of over 17,000 genes in more than 1,000 cancer cell lines obtained from high-throughput CRISPR-Cas9 viability screens. Gene essentiality captures the change in cell viability following targeted CRISPR-Cas9 knockout. Essential genes are critical for cell survival and proliferation in specific molecular contexts. Similarly, studies like GDSC⁶, CCLE⁷, CTRP⁸, and PRISM⁹ have measured the impact of various compounds on cancer cell line viability. Drug response experiments involve exposing cancer cell lines to varying concentrations of compounds and quantifying cell viability. These studies also gather deep molecular characterization of the cell lines, including RNA sequencing and whole-exome sequencing, defining the biological context. This enables the investigation of how molecular context influences cancer vulnerability and paves the way for more personalized medicine.

In this paper, we train machine learning models to predict perturbation responses from molecular profiles of the disease models in which they were tested. These approaches can be used to predict the impact of a perturbation in untested disease models^{10,11}, thus providing insights into the relevance of targets or compounds in different indications, disease models, or even patients. This capability can aid in prioritizing targets, compounds, or preclinical experiments in the early stages of the drug discovery pipeline.

Previous studies have proposed machine learning approaches for the prediction of gene essentiality¹⁰⁻¹² or drug response with promising performances¹³⁻¹⁸. Existing approaches can be classified into two categories: perturbation-specific (PS) and pan-perturbation (PP) models. Perturbation-specific models^{11,13-15} aim to predict the response of different biological systems to one specific perturbation using molecular data characterizing the disease model as input. If multiple perturbations are available in the data, as many perturbation-specific models can be trained. On the other hand, pan-perturbation models^{10,12,16-18} aggregate and leverage data from multiple perturbations. In this paper, we define a pan-perturbation model as a single-label regressor^{10,12,16-18} trained on all available pairs of disease models and perturbations to leverage features characterizing both the disease model (molecular data) and the perturbations

(fingerprints based on the annotated pathway of a genetic perturbation or the molecular structure of a drug). Note that a multi-label regressor predicting the response to multiple perturbations from the molecular profiles of the disease models could also be considered as a pan-perturbation model, but such models are omitted from the present paper as they have not been studied as extensively. Pan-perturbation models have the potential to uncover both mechanisms specific to a perturbation and those shared across perturbations. Unlike perturbation-specific models, pan-perturbation models leveraging perturbation descriptors can intrinsically predict responses to unseen (untested) perturbations, provided these can be appropriately represented. However, in this paper, we focus on predictions of responses to seen perturbations in unseen disease models, such as new cell lines, tissues, or more complex disease models like patient-derived xenografts (PDX). This ability to infer perturbation responses in diverse disease models remains a key need in drug discovery.

Among existing perturbation-specific models, TCRP¹¹ and CodeAE¹⁵ are designed to generalize beyond the training context. TCRP uses a model-agnostic meta-learning strategy to pre-train neural networks that can be quickly adapted to new tasks with limited data (few shots). The utility of TCRP has been demonstrated with pre-training in cell lines and fine-tuning in cell lines from an unseen tissue or in PDX. CodeAE, meanwhile, employs an autoencoder to align disease-model molecular data with patient data while handling potential confounding factors. Both approaches aim at robust generalization to new biological contexts, making them relevant benchmarks for our focus on “seen” perturbations in “unseen” disease models. We implement TCRP and report the performances obtained with both a pre-trained TCRP (zero-shot learning) for a fair comparison with other approaches, and a fine-tuned TCRP with 10 samples from the target domain (10-shot learning). However, we did not include CodeAE in our comparisons as the method was designed for classification instead of regression.

Recent pan-perturbation methods such as DeepDep¹⁰ for gene essentiality prediction, or tDNN¹⁸ and DrugCell¹⁷ for drug response prediction combine representations of disease models and perturbations. Our previous work, OmicsRPZ¹², improved gene essentiality predictions by first learning these two separate representations and then training a Light Gradient Boosting Model (LGBM) on these combined representations. We leverage and expand our work on representation learning, with a stronger focus on the choice of prediction model.

Although pan-perturbation models generate promising results, and despite the fact that they are often trained on a large amount of data including multiple perturbations, it remains unclear whether they outperform perturbation-specific models to predict the response to a known perturbation in a new biological context^{18,19}. In addition, pan-perturbation models often require more parameters than perturbation-specific approaches as they distinguish both diverse perturbations and biological contexts, which leads to a more complex training and hyper-parameter tuning. In this paper, we propose Layered Ensemble of Autoencoders and Predictors (LEAP) (Figure 1), a novel perturbation-specific approach to predict perturbation response using gene expression data. For each perturbation, LEAP uses an ensemble of perturbation-specific LASSO regressors trained in multiple random subsamples of cell lines with diverse gene expression representations. Those representations are obtained from randomly

initialized Data Augmented Masked Autoencoders (DAMAE). We pre-train the autoencoders using unlabelled data on various disease models (cell lines and PDX) to capture common biological patterns and reduce computational time. LEAP leverages (i) recent advances in deep representation learning, which have achieved state-of-the-art results in various domains, and (ii) model ensembling, which enhances prediction precision and robustness by utilizing model randomized diversity^{20–22}.

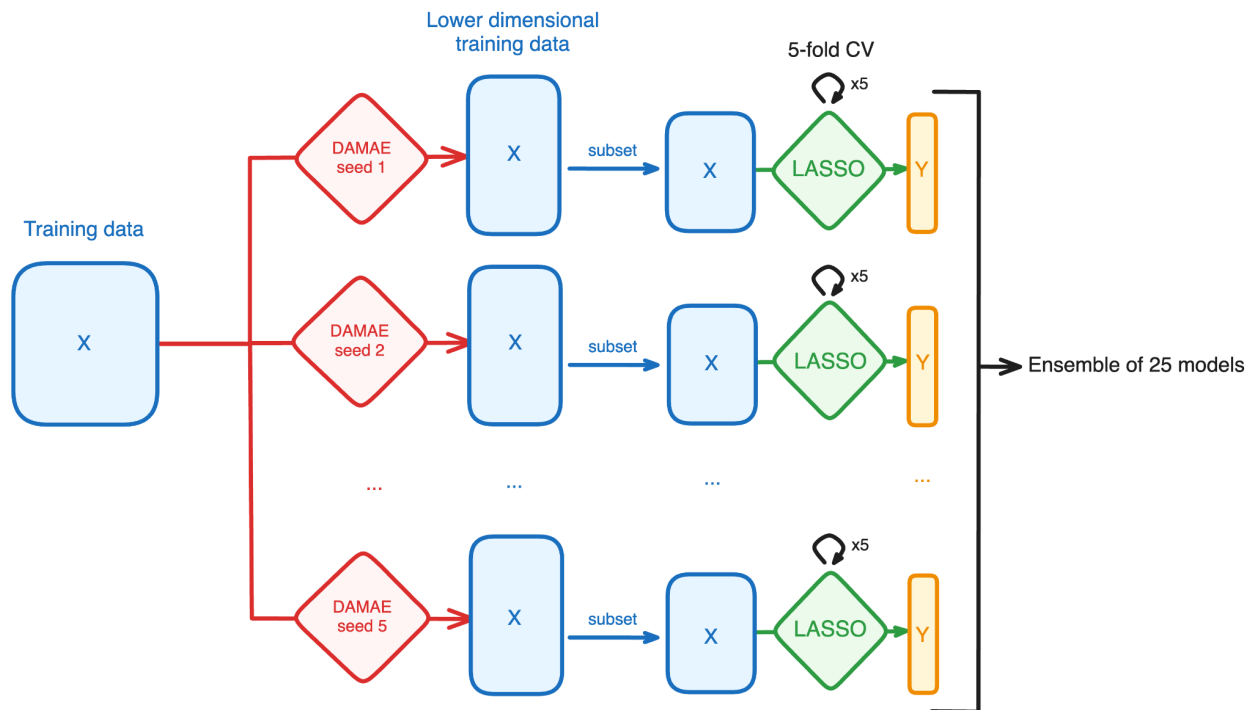


Figure 1. Illustration of LEAP. The training data is first transformed using five DAMAE models that have been trained with different random seeds. We use a 5-fold cross validation on each of the five representations of the data and ensemble the five regressors trained on the different cross validation folds with the best performing hyper-parameters.

We evaluate the performance of our approach in gene essentiality prediction using the same setup as the DeepDep¹⁰ and OmicsRPZ¹² studies. We extend our evaluation to various tasks studied in the literature including both gene essentiality and drug response prediction in unseen cell lines, unseen tissues and unseen disease models. We use the latest available release of the datasets, and we standardize the training and evaluation framework between gene essentiality and drug response tasks. We compare ourselves to existing methods on previously proposed tasks when possible. In line with previous publications^{15,23–26}, we consider that drug discovery operates within a transductive framework, which implies that unlabelled test data (e.g. RNAseq profiles) are available during training. This can be leveraged by pretraining the representation model on both labelled and unlabelled data with limited impact on the prediction performances, as demonstrated in our ablation studies. In this paper, we pre-train DAMAE representation models on all available RNAseq data and compare prediction performances obtained using different regression approaches on the same data representation.

We show that LEAP significantly outperforms recent existing approaches in predicting gene essentiality in unseen cell lines. Furthermore, LEAP yields better prediction performances than state-of-the-art pan-perturbation models in unseen cell lines and tissues. Notably, we show in an ablation study that the ensembling of different data representations in LEAP outperforms methods that ensemble prediction models alone.

Results

Outline

We propose LEAP, a novel approach to predict perturbation response (gene essentiality or drug response) in a disease model based on gene expression before perturbation (Figure 1). We use publicly available data from perturbation experiments conducted in cell lines in the DepMap⁵ and PharmacnoDB²⁷ studies, and in Patient-Derived Xenografts (PDX) in the PDX Encyclopedia²⁸ (Supplementary Table 1, Supplementary Figure 1). We consider three challenges, where we aim to predict perturbation response in (i) unseen cell lines, (ii) cell lines from an unseen tissue of origin, or (iii) unseen PDX (Table 1).

Challenge	Task id	Label	Data	Number of cell lines	Number of perturbations	Number of (cell line, perturbation) pairs
i - Prediction in unseen cell lines	1a	Gene dependency	DepMap (version 23Q4)	1,019	1,539	1,568,222
	1b	Gene dependency	DepMap (OmicsRPZ ¹²)	893	1,223	1,092,139
	2a	Drug response (AAC)	PharmacnoDB	1,399	649	551,024
ii - Prediction in unseen tissue of origin	3a	Gene dependency	DepMap (version 23Q4)	1,019	1,539	1,568,222
	3b	Gene effect	DepMap (version 18 ²⁹)	335	469	157,115
	4a	Drug response (AAC)	PharmacnoDB	1,399	580	528,463
	4b	Drug response (AUC)	GDSC v1	951	194	166,848
iii - Prediction in unseen disease model	5a	Drug response	PharmacnoDB, PDX	1,390 (140 PDX)	5	6,129 (227 PDX)

	(AAC)	Encyclopedia			
--	-------	--------------	--	--	--

Table 1. Task description. For each of our eight tasks, we report the type of label to predict, dataset version, number of cell lines, number of perturbations and number of pairs of cell lines and perturbations. Tasks "a" correspond to our main tasks using the latest releases of the datasets, while tasks "b" have been designed in an attempt to compare ourselves with published results.

LEAP builds upon our previous pan-perturbation approach OmicsRPZ¹², which proposed SOTA models to predict gene essentiality alongside a rigorous benchmark strategy. We use a lower-dimensional representation of the gene expression data obtained by combining the two best performing approaches identified in this previous work into a Data-Augmented Masked Auto-Encoder (DAMAE). To reduce computational burden and ease hyper-parameter tuning, we use multiple perturbation-specific LASSO regressions instead of a pan-perturbation model as previously proposed^{10,12}. We tune the hyper-parameters of each regressor by maximizing Spearman's correlation using a 5-fold cross-validation within the training set. We design a layered ensembling strategy aimed at enhancing the robustness of both the data representation and the prediction model. To do so, we propose a two-layer randomization and ensemble learning strategy (Figure 1). We train five DAMAE models with different random initializations on the same large dataset combining RNAseq data from all available cell lines and PDX samples. We then train regression models on the five different data representations generated by the DAMAEs. For the first layer of ensembling, we aggregate the predictions from five regression models that are trained on the splits of the 5-fold cross-validation used to tune the model hyper-parameters. For the second layer of ensembling, we aggregate the predictions of the five sets of regressors obtained with different data representations. In total, LEAP ensembles 25 regression models trained on five different data subsets of five different data representations.

We compare our novel approach LEAP with published pan-perturbation models, including DeepDep¹⁰ and all models trained in the OmicsRPZ¹² study on the gene dependency prediction in unseen cell lines (challenge i, task 1b). We also compare LEAP with six approaches where the regressors are trained using gene expression data represented by the same DAMAE model that we introduced in the present paper. We considered three pan-perturbation (PP) models, including PP-LGBM, which is an update of the best model from OmicsRPZ using our DAMAE model, PP-tDNN¹⁸ and PP-MLP, and four perturbation-specific (PS) models, including the baseline PS-KNN, PS-LASSO, PS-LGBM and PS-TCRP (for out-of-domain prediction tasks only).

LEAP improves perturbation response predictions in cell lines

In our first task, we predict gene essentiality in unseen cell lines using the same data and evaluation framework as in OmicsRPZ¹². LEAP outperforms all approaches proposed in OmicsRPZ with different representation models and yields an increase in average per-perturbation Spearman's correlation of 16% (0.256 to 0.297) compared to the best OmicsRPZ model (Figure 2, Supplementary Table 2). LEAP outperforms all other approaches, including the perturbation-specific and pan-perturbation models using the DAMAE

representations, in terms of both per-perturbation and overall Spearman's correlation (Supplementary Figure 2, Supplementary Table 2). For subsequent analyses, we focus on per-perturbation metrics to evaluate the ability of the model to select the most responsive samples for a given target or drug, a critical need in precision medicine. This metric is preferred by many of the recent publications^{11,12,14,15} (see Discussion).

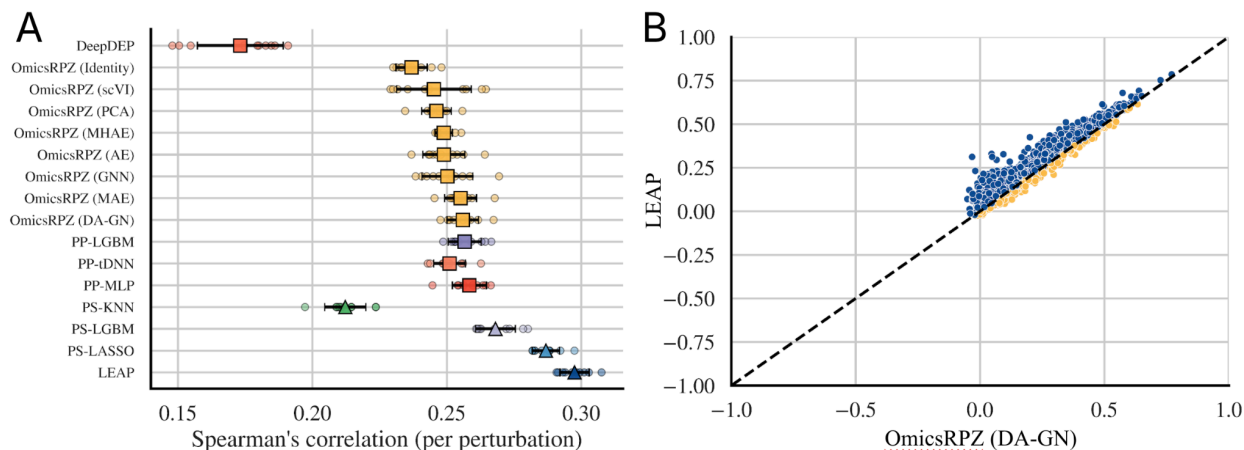


Figure 2. Comparison of the performances in predicting gene dependency in unseen cell lines using LEAP or existing approaches (task 1b). We compare the performance of our approach (LEAP) with previously reported performances obtained in DeepDEP¹⁰, using different representation models in OmicsRPZ¹², and re-implemented baseline and state-of-the-art approaches. Models are evaluated for the 1,223 gene perturbations included in the OmicsRPZ study over 10 repeated holdout test sets of unseen cell lines. (A) Boxplots for different models where each point indicates the average Spearman's correlation coefficient over the 1,223 gene perturbations obtained in each of the 10 test sets. (B) Per-perturbation performances obtained using the best model from OmicsRPZ (x-axis) or using our model (y-axis). We report the average Spearman's correlation of each perturbation over the 10 test sets. Note that the performances of OmicsRPZ model were not recomputed and were obtained with different training-test splits of the same dataset.

We update the data used in this task using a more recent release of the data and focusing on the prediction of the 1,539 dependencies of interest with the largest variance (Table 1). Similarly, LEAP outperforms all other approaches and yields an increase in Spearman's correlation of 17% (0.284 to 0.332) compared to the latest state-of-the-art approaches (Figure 3A, Supplementary Table 3), with a lower computation time (<1 hour for LEAP, compared to 35 hours for PP-LGBM on ml.m6i.32xlarge, excluding DAMAE training time, which is <1h for 5 AE on ml.g5.24xlarge).

Our results are consistent for the prediction of drug response in task 2a, where we observe an increase in Spearman's correlation of 4% (0.335 to 0.350) compared to the PP-LGBM (Figure 3B, Supplementary Table 3). LEAP also outperforms all other models in the external validation study (Supplementary Figure 3). The prediction performances obtained with LEAP are close to the drug response measurement reproducibility across studies (Supplementary Figure 3).

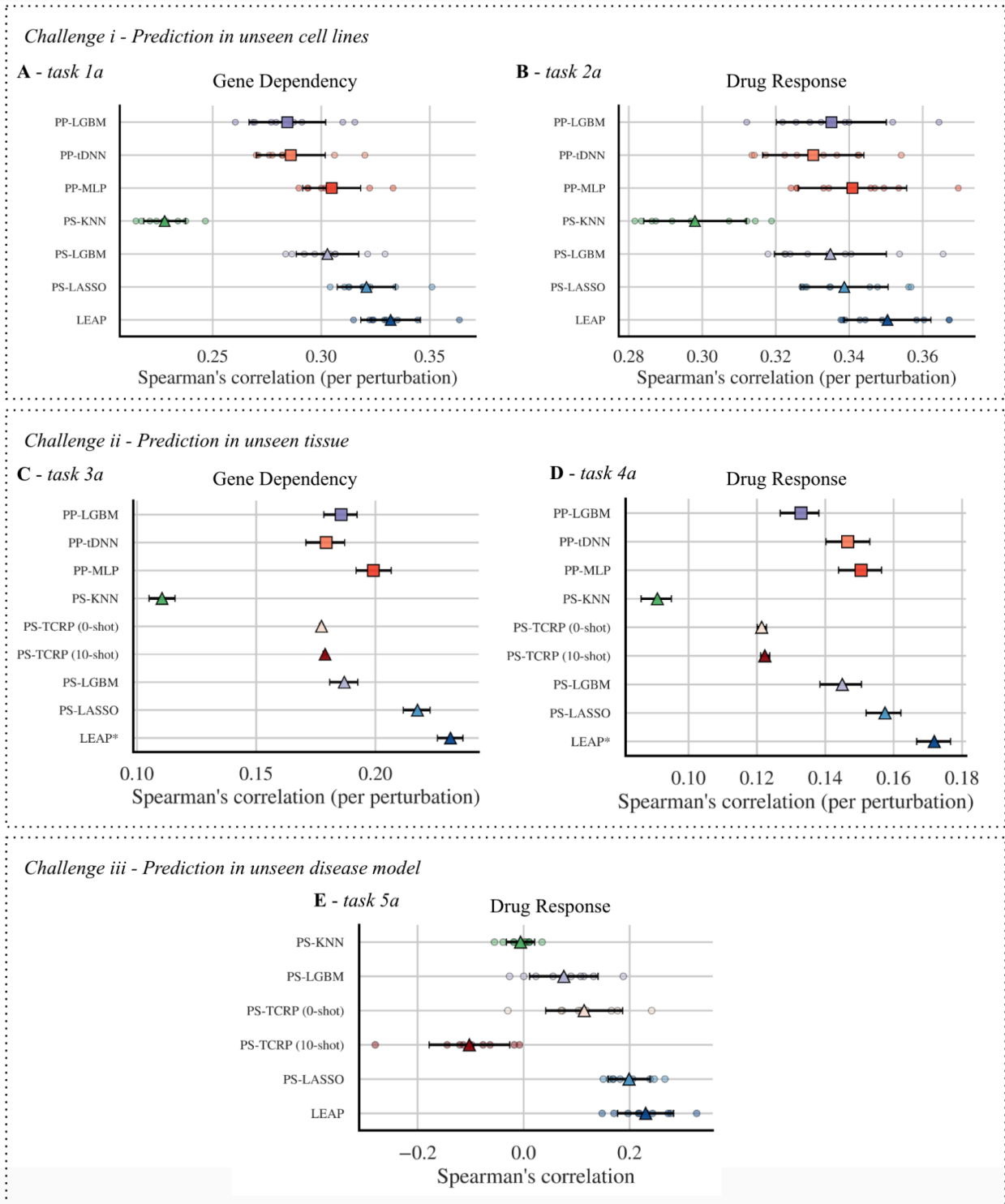


Figure 3. Performances in predicting perturbation response in unseen cell lines or cell lines from an unseen tissue of origin. We compare the performances of our novel approach (LEAP, in blue) with a baseline model (PS-KNN, in green) and state-of-the-art models (PP-LGBM and PS-LGBM in purple, PP-tDNN in orange, PP-MLP in red). We evaluate the performances in predicting **A** gene dependency in unseen cell lines, **B** drug response in unseen

cell lines, C gene dependency in an unseen tissue, and D drug response in an unseen tissue. Performances are evaluated over 10 repeated holdout splits (A, B) or by sequentially using each tissue as a test and bootstrapping the results to obtain confidence intervals (C, D).

The perturbation-specific and ensembling frameworks improve performances in LEAP

We evaluate the impact of each of our methodological choices on the prediction performance in an ablation study (Supplementary Table 4, Supplementary Figure 4). The largest performance increase of 14% (from 0.282 to 0.322) is observed when using perturbation-specific LASSO regressions (PS-LASSO) instead of a pan-perturbation LGBM (PP-LGBM) (Supplementary Figure 4).

We distinctly evaluate the gain in performance due to the first and second stages of our ensemble learning strategy in this ablation study (Supplementary Table 4, Supplementary Figure 4). The ensembling of the five regressors trained on the splits of the 5-fold cross validation (first stage ensembling) yields an increase in performance of 1% (0.318 to 0.321) compared to the use of a single regressor trained on the full training set. Further ensembling the 25 regressors trained on 5 different data representations (second layer ensembling) yields a larger 3% (0.321 to 0.332) increase in performance (Supplementary Figures 4 and 5).

To further assess the relevance of the second stage ensembling, we compare the performance of LEAP with an ensemble of 25 LASSO regressions trained on different subsets of the same deep representation (Supplementary Table 5). The ensembling of 25 regressors trained on the same data representation yields a very limited increase (below 1% - 0.321 to 0.322) in performance compared to the ensembling of 5 regressors only. This suggests that the larger gain in performance in LEAP is due to the use of multiple data representations in the second stage ensembling and not only to the larger number of regressors that are ensembled.

Of note, we observe a limited decrease lower than 1% (0.321 to 0.319) in Spearman's correlation when training the DAMAE on data from all cell lines instead of using the training data only (Supplementary Table 4, Supplementary Figure 4, Discussion).

LEAP generalizes better in unseen tissues

In tasks 3 and 4, we aim to predict perturbation response in cell lines from an unseen tissue (Table 1). To improve the performance of LEAP on unseen tissues, we tune the hyper-parameters using a grouped 5-fold cross-validation where cell lines of the same tissue are part of the same split.

As before, we observe better performances in predicting gene essentiality or drug response with LEAP compared to all other approaches, resulting in an increase in Spearman's correlation compared to the latest state-of-the-art PP-LGBM of 23% (0.190 to 0.233) and 31% (0.130 to 0.170) respectively in tasks 3a and 4a (Figure 3D-E and Supplementary Table 3). LEAP

outperforms other approaches consistently across all tissues, except Myeloid and Head/Neck in task 4a (Supplementary Figure 6). The use of a grouped cross-validation by tissue instead of classical cross-validation yields a limited improvement of 3% for LEAP (0.165 to 0.170) in Spearman's correlation for the drug response task 4a only (Supplementary Table 6). LEAP shows a better relative improvement on these out-of-domain tasks (23%, 31%) compared to the other models than in the prediction of perturbation response in cell lines (16%, 17%, 4%). Results are consistent in tasks 3b and 4b, which correspond to previous versions of the data (Supplementary Figure 7).

Transfer to different disease models

Task 5 evaluates the transferability of our models from cell lines to more complex disease models, namely patient-derived xenografts (PDX) in mice. Zero-shot models, including LEAP, are trained in cell lines and used to predict the change in tumor size after drug administration in PDX based on their RNAseq profiles. The 10-shot TCRP¹¹ model is fine-tuned using data from 10 PDX samples. LEAP outperforms all other models in predicting drug response in PDX (Figure 3E, Supplementary Figure 8). Surprisingly, we observe no increase in performance with fine-tuning, contrary to what was reported in the original paper and potentially due to inherent challenges in directly comparing performance with the TCRP model, including differences in input modalities (RNAseq vs. microarray) and definition of the splits. Further investigation is needed to fully assess the feasibility and limitations of this transfer, as well as to refine the task definition for future studies.

Discussion

LEAP yields better performances than existing models in predicting gene essentiality or drug response in unseen cell lines or tissues in all of our tasks. We obtained average Spearman's correlations of 0.33 and 0.35 for the prediction of gene essentiality and drug response respectively in unseen cell lines. Previous publications^{30,31} reported issues in measurement reproducibility between studies, with Pearson's correlations between measured responses in different studies varying between 0 and 0.8 depending on the drug and studies. Although some of the technical differences between studies have been corrected analytically in the R package PharmacoGx, we observed an average Spearman's correlation in drug response between 0.2 and 0.25 between our training studies (GDSC, CTRP and CCLE) and PRISM, which defines an upper bound on achievable prediction performance due to inherent variability across datasets. We demonstrated that our drug response prediction performances are on par with label reproducibility between our training studies and PRISM.

Our ablation study shows that the largest increase in prediction performance compared to PP-LGBM is due to the use of perturbation-specific models in LEAP. We also demonstrate that the ensembling of regression models trained on data representations obtained with multiple DAMAE models generates an increase in performance compared to the ensembling of the same number of regressors trained on a single representation. This suggests that the

stochasticity of deep learning representation models can provide robustness and capture complementary patterns. Indeed, RNA-seq data presents unique challenges, including high noise levels and strong correlations between features, making it difficult to apply data augmentation techniques commonly used in other domains. To address this, we incorporated masking, noise-based data augmentation and ensembling to enhance the robustness of our molecular data representation. We believe that this representation learning ensemble framework could be beneficial in other machine learning tasks, including for instance predictions from histology slides. In LEAP, we use five DAMAE models that have been trained on all available unlabelled samples to transform the data before training the regression models. This has two main advantages. First, the use of pre-trained representation models instead of training the representation model on each training set reduces the computational time. Second, the representation model can be trained on a larger and more comprehensive RNAseq dataset. In this paper, we leverage a larger publicly available RNAseq data from cell lines and PDX models that did not necessarily have perturbation responses available.

To evaluate the prediction performances of LEAP and other approaches, we defined 5 tasks including the prediction of gene essentiality and drug response in unseen cell lines or tissues. All tasks use publicly available data, which makes them easily reproducible. In gene essentiality tasks, we restrict our prediction to the 1,539 dependencies of interest with largest variance to discard the genes that are essential in all or none of the cell lines. We use multiple training-test splits to account for the variability in performances due to data splits as previously proposed¹². We include comparisons of LEAP with previously proposed methods in supplementary tasks that were designed to be as similar to previous settings as possible in terms of data version, label, perturbations included and number of cell lines (Table 1). Despite the fact that previous approaches were applied to data from the same studies, exact comparisons were challenging and we could not replicate some of the published results due to changes in the selection of perturbations and cell lines, as well as the use of different input modality (e.g. RNAseq, microarray, mutations), preprocessing methods, readouts, performance metrics, or training-test splits³². To facilitate such comparisons in the future, we make the code and data used in this paper publicly available and encourage the use of the same evaluation pipeline and tasks.

While calibrating models across different targets and compounds is valuable in drug discovery, our primary focus is on optimizing predictions within individual perturbations to better identify treatment responders. To mimic this real-world drug discovery need, we prioritize per-perturbation metrics, ensuring a practical approach for patient selection. This focus also allows us to make our study comparable to existing perturbation models, such as TCRP¹¹, OmicsRPZ¹², CodeAE¹⁵, and Velodrome¹⁴, which similarly emphasize identifying the best responders to specific perturbations. Previous studies also sometimes reported an overall correlation comparing the responses (or rankings) over all pairs of perturbations and disease models. We argue that such overall metrics may not be appropriate as they primarily capture differences between the perturbations³³. Indeed, it has been shown that a pan-perturbation model trained with randomized RNAseq data performs similarly to a pan-perturbation model using real RNAseq data in terms of overall correlation³³. This suggests that the signal recovered is mainly used to classify perturbations rather than capturing the biological signal from each

perturbation. Hence, per-perturbation metrics are better suited to evaluate the ability of the model to capture meaningful biological insights, improve predictive performance for individual perturbations, and eventually improve translatability in drug discovery pipelines. Correlation metrics are particularly relevant when labels differ in scale, as in Challenge III. However, small variations in perturbation responses can affect correlations, even when the meaningful range of responses is preserved, potentially leading to a misinterpretation of performance. To address this, we focus on dependencies with high variance and report Mean Squared Error (MSE) as an additional performance metric.

More generally, our results suggest that perturbation-specific models can outperform more complex pan-perturbation models in predicting the response to a seen perturbation in an unseen biological context. Although pan-perturbation models take additional information as input (perturbation fingerprints), we hypothesize that their weaker performances here are due to (i) the use of a global loss, making the model potentially focusing more on perturbations with larger variance and on the discrimination between perturbations, and (ii) a more challenging tuning. On the other hand, perturbation-specific models are computationally faster to train, less challenging to tune, and do not require the availability of fingerprints, which represents extra work and can pose difficulties when integrating various types of perturbations (e.g., gene, small molecules, antibodies). Pan-perturbation models remain promising thanks to their ability to leverage data from other perturbation experiments, which could be useful when a perturbation has only been tested in a limited number of disease models. We recommend that future research consistently compares pan-perturbation models to perturbation-specific models like LEAP to ensure that they offer added value.

In our evaluation framework, the label (perturbation response) from the test set is unseen, but the features (RNAseq) are seen during representation model training. Given new RNAseq data where perturbation responses are unknown, our unsupervised DAMAE models can be retrained on all available RNAseq data, including both labelled and unlabelled samples, as in CodeAE¹⁵. This reflects the transductive nature of the task we consider in this paper. Overall, DAMAE training on all samples or only training samples has a limited impact on prediction performances. In our ablation study, we observed a small decrease in prediction performance when using DAMAE models trained on all samples instead of training samples only. We hypothesize that this small decrease in performance is due to the fact that a DAMAE trained on all samples learns features that may be underrepresented in the training set and cannot be exploited by the regressors, leading to a poorer generalization of the model on the test set.

Our study has a number of limitations. First, the hyper-parameter tuning is based on grid search using restrictive grids for all approaches and some of the hyper-parameter choices could be further explored (e.g. dimensionality in DAMAE). This could be improved in future work by expanding the hyper-parameter search space and using a better optimized parameter sampling algorithm, provided that the computational budget is increased. Similarly, parameters that relate to the processing and representation of gene expression data could be further tuned for the specific task of perturbation response: representation dimension, normalisation, scaling, gene selection. For those parameters, we adhere with parameters selected in previous work¹².

Second, we use a simple ensembling strategy by calculating the unweighted average of predictions from multiple regressors in LEAP. Performances could potentially be improved by using a weighted average based on the performances of individual regressors, more complex ensembling techniques (e.g. routing or boosting), or a different number of ensembled models. Third, we use established perturbation fingerprints for the pan-perturbation models. Perfecting these representations may improve the performances of pan-perturbation models. Fourth, even if the hyper-parameter selection of pan-perturbation models is dictated by per-perturbation metrics, their loss and consequently their optimization rely on a global loss over all perturbations and preclinical models, which may be detrimental to their final performance. Fifth, all models presented in the present paper only use gene expression profiles as input. Although previous work suggested that gene expression is the most informative modality to predict perturbation response¹⁰, additional data modalities, including mutations and protein expression, are available and could be leveraged to better characterize the cell lines. Sixth, there are known intrinsic differences between the molecular profiles of cell lines and PDXs. In particular, previous work suggests that the gene expression in PDX is closer to the one in tumors than the gene expression in cell lines, as cell lines suffer from the lack of cell diversity, tumor micro-environment, and sometimes high passage numbers³⁴. Although we aim at exploring the generalization capabilities of LEAP by evaluating models trained on cell lines data on PDX, those known differences may partially explain the lower performances on this task. Future work could focus on the extension of LEAP with transfer learning approaches to improve its performances in out-of-domain data, including in unseen tissues, disease models or even patients. Our method could also be adapted to predict binary labels, which would allow us to compare ourselves to CodeAE¹⁵. This may be beneficial to be less sensitive to noise in the data and learn common patterns across the different treatment response metrics that are used in cell lines, PDX and patients.

Conclusion

We have proposed LEAP, a new perturbation-specific model leveraging both ensembling methods and deep representations of expression profiles. Our model outperforms state-of-the-art models for gene essentiality and drug response prediction in all our tasks. Our model has minimal tuning requirements to facilitate broader and more effective applications in the prediction of perturbation response. We believe that our approach could accelerate the discovery, positioning and repurposing of anti-cancer therapies to ultimately improve patient outcomes. We make our code and evaluation pipeline available for future research.

Materials and Methods

Datasets

This study is based on publicly available data from DepMap, PharmacDB and PDX Encyclopedia ([Supplementary Table 1](#)).

DepMap

CRISPR knockout screens on human cancer cell lines and related omics datasets are downloaded from DepMap 23Q4. Perturbation screens' outcomes are obtained from the project Achilles³⁵, and processed by DepMap⁵ through a pipeline^{29,36} using Chronos³⁷ on each screen library to output gene effect scores. For every studied gene representing a dependency of interest, gene effect scores are then aggregated and corrected per cell line to generate gene dependency scores. Both scores are available on the DepMap platform. Our study focuses on the gene dependency score as it measures the probability that a gene is essential for the survival of a particular cell line. Gene expression data is obtained from CCLE³⁸ via the DepMap portal. We use the publicly available transcripts per million (TPM) normalized counts as cell lines descriptor inputs for our models.

For task 1b and comparison with OmicsRPZ¹², gene dependency data and TPM gene expression data are downloaded from DepMap 22Q4³⁹. Perturbation outcomes and omics originate from the same sources and pipelines, without corrections added in 23Q4, but do not cover as many cell lines as in later versions.

For comparison with TCRP¹¹, in task 3b, gene effect data is downloaded from the first release of DepMap in 2018²⁹. However, in this same task, we use the TPM gene expression data from the 23Q4 release.

PharmacDB

Drug perturbation screens on human cancer cell lines are downloaded from PharmacDB²⁷ using the R package PharmacGX (version 3.4.0)⁴⁰. From the 15 studies that are accessible through PharmacGX, we retain CCLE-2015, GDSC-2020 (v1-8.2 and v2-8.2), CTRPv2-2015 and PRISM-2020 which are respectively referred to as CCLE, GDSC (v1 and v2), CTRP and PRISM. The tested drugs (Supplementary Table 1) cover a wide range of anti-cancer drugs including cytotoxic agents (paclitaxel, bendamustine) and targeted therapies (erlotinib, everolimus, ruxolitinib), and range from experimental molecules to clinically-approved drugs. For the different learning tasks, we use the area above the dose-response curve (AAC) which is measured on a drug-specific dose range. A high AAC shows a high average efficacy. For tasks 4b and 5b, the area under the drug-response curve (AUC) is downloaded directly from the GDSC study⁴¹.

Gene expression data before perturbation is downloaded with PharmacGX when available, which is only the case for some of the cell lines studied in GDSC (v1 and v2) amongst the retained studies. For other studies or cell lines without gene expression data in GDSC (v1 and v2), we use the gene expression data from DepMap 23Q4.

PDX Encyclopedia

Drug response screens in patient-derived xenografts (PDX) are obtained from PDX Encyclopedia²⁸. Of the 63 available perturbations, we restrict our analyses to the five

mono-therapy drugs that were studied previously¹¹: Paclitaxel, Cetuximab, Erlotinib, Tamoxifen and Trametinib. Drug response is provided as the minimal percentage of tumor volume change observed over 10 days of treatment. We download available gene expression raw counts.

Perturbation fingerprints

In the pan-perturbation model approach, perturbations' encodings are required as a unique model learns and predicts the outcome of diverse perturbations. In practice, such models use gene and drug biological or molecular descriptors (also called fingerprints) to better capture similarities between perturbations⁴².

Gene fingerprints

We use gene fingerprints derived from the Molecular Signatures Database (MSigDBv6.2⁴³) that describe the affiliation of each gene (dependency of interest) in gene sets that are up or down-regulated in response to a perturbation experiment. Most of those signatures are curated from the literature. Gene perturbations with similar fingerprints tend to be activated or repressed together in perturbation experiments included in the Molecular Signatures Database. We use the same 3115 chemical and genetic perturbations (CGP) curated gene sets as in DeepDEP¹⁰, which were obtained after filtering out the 318 sets that do not involve any of the 1298 genes studied in their paper.

Drug fingerprints

Drug fingerprints are solely based on their molecular composition. Every drug perturbation name obtained from PharmacDB²⁷ or PDX Encyclopedia²⁸ is mapped to its corresponding Compound Identifier (CID) on PubChem via the PubChem API⁴⁴. Canonical Simplified Molecular Input Line Entry System (SMILES) are then downloaded from the compound card and further processed with the github repository CDDD⁴⁵ and the rdkit package ("RDKit: Open-source cheminformatics") to remove salts and stereochemistry from the SMILES sequence. Additionally, we kept existing filters in the CDDD package that filter out molecules based on their molecular weight, number of heavy atoms or partition coefficient. Morgan fingerprints are then generated from SMILES with rdkit as vectors, using a radius of 2 and a size of 2048.

As the SMILES are downloaded from PubChem, perturbations that are combinations of compounds or drugs that do not match to any CID (lack of matching terms, inexistence of a compound card for compounds in early development stages) cannot be encoded with fingerprints and are excluded from tasks that compare the performances of pan-perturbation versus perturbation-specific model approaches.

Data preparation

Sample and perturbation selection

Overall, the data curation of DepMap⁵, PharmacoDB²⁷ and PDX Encyclopedia²⁸ is done in two steps where (i) we keep samples with available RNAseq data, information on the tissue of origin and exclude outliers, (ii) we select the perturbations that will be investigated (Supplementary Figure 1). For PharmacoDB, we have an additional final step to remove duplicated sample-perturbation pairs arising when combining data from GDSC, CCLE and CTRP.

DepMap. For our main tasks, we use the version of DepMap released in Q4 of 2023 (version 23Q4). We drop 79 DepMap cell lines with no available RNAseq data (Supplementary Figure 1A). Two outliers are then identified in the DepMap data by visually inspecting the first principal components obtained from a Principal Component Analysis (PCA) of the RNAseq data. After excluding these outliers, we define a new list of dependencies of interest with standard deviation of the gene dependency above 0.2¹⁰, resulting in 1,593 dependencies

PharmacoDB. We first prepare the data from each of the five retained studies individually (Supplementary Figure 1B). We only keep the drugs with available fingerprints to allow for the comparison of different modeling approaches (see below). We then remove duplicated responses measured for the same drug in the same cell line across the five studies. More precisely, within each single study, when the same drug is tested multiple times on the same cell line, we aggregate the observations by taking their median response. This operation helps reduce uncertainty and noise in experiments performed in the same study. Later, if the same drug is tested on the same cell line in different studies, observed outcomes are not aggregated across those studies as experimental setups such as concentration ranges may vary. Therefore, we keep only one of the studies' outcomes by taking the first appearance of the experiment based on an arbitrary order of the studies: GDSC v2, GDSC v1, CCLE, CTRP and PRISM. Unless a precise study is explicitly mentioned, we refer to the aggregation of the 4 datasets GDSC v1, GDSC v2, CCLE and CTRP as PharmacoDB. For all learning tasks, we only retain drugs that are administered to at least 75 cell lines. We use PRISM as an external validation set and retain drugs that are administered to at least 15 cell lines in this dataset.

PDX Encyclopedia. We keep the 140 PDX with available RNAseq and drug response data (Supplementary Figure 1C). Of the 63 treatments tested in the study (including 25 combinations of drugs), we only keep the 5 drugs that were also administered to cell lines in the PharmacoDB dataset ¹¹.

For comparison with previous studies, we also reproduced some of our analyses using former versions of these datasets. These include (i) the DepMap (OmicsRPZ) dataset with 893 cell lines and 1,223 dependencies of interest used in OmicsRPZ¹², (ii) DepMap (version 18) with 335 cell lines and 469 dependencies of interest²⁹, and (iii) the AUC data reported by GDSC with 951 cell lines and 194 drugs for comparability with the CTRP publication ¹¹.

RNaseq data preprocessing

We downloaded TPM counts from DepMap⁵ and transformed raw counts into TPM normalized counts using an in-house software package for GDSC⁶ and PDX Encyclopedia²⁸. TPM counts are then log₂-transformed with the addition of a pseudo count of 1. We keep the 5,000 most variant genes in each of the three datasets separately, which results in a total of 7,083 unique genes. We standardize the TPM counts, so that each gene expression has a mean of zero and a standard deviation of one.

Tasks

We define three types of challenges, where we aim to predict perturbation response in (i) unseen cell lines, (ii) an unseen tissue, or (iii) an unseen disease model (Table 1)¹¹.

Challenge I: prediction in unseen cell lines

The first challenge encompasses two tasks that focus on predicting the response of a new cell line to a perturbation (a gene knockout or a drug) already performed on other cell lines. From a clinical perspective, this challenge mimics a key approach in precision oncology: to determine if a new patient would respond to a therapy that was already tested in other patients.

The first task consists in predicting gene dependency in unseen cell lines using the DepMap⁵ dataset. For this, we train and evaluate models to predict the dependency of each of the 1,539 genes defined above using the 23Q4 release of the DepMap dataset that was curated as described above (task 1a). For an exact comparison with OmicsRPZ¹², we also implemented an alternative version of this task using the same version of the DepMap dataset that was used in OmicsRPZ (task 1b) we aim to predict the dependency of 1,223 genes.

The second task focuses on the prediction of drug response (AAC) in unseen cell lines using the PharmacDB²⁷ dataset (task 2a). Following recent recommendations⁴⁷, we focused on AAC instead of other measures like IC₅₀. The models are trained and evaluated in GDSC v2 and v1, CTRP and CCLE, and we keep PRISM as an external test set. We predict the response to the 648 drugs available in the training set (GDSC, CTRP and CCLE) that are administered to at least 75 cell lines (Supplementary Figure 1). The evaluation of performances in PRISM is restricted to the 254 drugs that are also included in the training data.

To evaluate the prediction performance of the different modeling approaches, we use a repeated holdout cross-validation framework¹². The data is split into a training set with 80% of the cell lines and a test set with the 20% remaining cell lines. This procedure is repeated 10 times to increase the robustness of the evaluation.

Challenge II: prediction in an unseen tissue

The second challenge comprises two tasks that aim at inferring the response to perturbation (a gene knockout or a drug) in cell lines originating from a tissue that is not observed in the training

set (Table 1). This challenge could be seen as a drug repurposing task, where we aim to evaluate if an existing drug might be effective for a new indication or a different subpopulation of patients. It is also valuable for target identification and validation, especially when genes or drugs have been screened across various cell lines, but not specifically in the tissue of interest. For instance, in DepMap⁵, only 24 cell lines are available as a proxy for mesothelioma, and only 3 of sarcomatoid type. These out-of-domain tasks are more arduous as models aim to predict in cell lines with tissue-related molecular specificities that are not seen at training time.

For the gene dependency task 3a, the out-of-domain capabilities of the different models are assessed on each of the 18 tissues with more than 25 cell lines available in the latest DepMap data, so that there is always a minimum of 10 cell lines available for few-shot learning, and 15 cell lines for computing a performance metric. In an effort to compare our results with previous studies, like TCRP¹¹, we also use gene dependency scores from DepMap version 18 (task 3b). In task 3b, we aim to predict the gene effect of each of the 469 genes with the highest absolute standard scores, meaning that those genes are the ones whose gene effect in at least one cell line is the furthest in standard deviations from the mean. Using the same selection criteria as in task 3a for tissues, we compare the performance of the different models on 5 tissues. Note that we could not recover the exact same dataset that was used in the other study as the lists of cell lines and dependencies of interest were not provided. Applying the same threshold of 6 for standard scores leads to the selection of 428 genes. A reusability report³² points out challenges in obtaining the exact data used by TCRP, therefore preventing achieving the exact same performances when trying to reproduce the results.

For drug response, we first keep the 10 tissues with the largest sample size in the PharmacDB²⁷ data (task 4a). The tissue selection slightly differs from tasks 3a and 3b as most drugs are not tested in all cell lines, which requires us to set a threshold on both the number of tissues and the number of cell lines tested for each drug within a tissue to select test cases. As a result, we use the 525 drugs that were tested in at least 25 cell lines for each of these 10 tissues (see supplemental material). For comparison with previous studies¹¹, in task 4b we use the GDSC data only and aim to predict the AUC (instead of AAC in previous drug response tasks) for 190 targeted drugs.

We evaluate prediction performance in cell lines from the tissue of origin that was not used in the training set. To evaluate variability, we create 1,000 test sets by repeatedly removing 10 cell lines from the target tissue at random (for computational reasons, for TCRP we only analyze 10 repeats). We repeat this procedure such that each tissue is in turn considered as the target tissue. We report the tissue-specific performances (average of the per-perturbation performance on a given tissue over all perturbations) as well as the average performance over all unseen tissues.

Challenge III: prediction in an unseen disease model

Challenge 3 aims to evaluate the ability of the models trained in cell lines to generalize to other disease models (Table 1). For this, we first train the models to predict drug response using all available cell lines in the full PharmacDB²⁷ dataset (task 5a), or in GDSC only (task 5b) for

comparison with previous results¹¹. These models are then used to predict the negative minimum change in tumor volume compared to the pre-treatment baseline over a 10-day post-treatment period measured in PDX treated with the same drug.

To assess variability and be as comparable as possible to published results¹¹, we evaluate prediction performance over 10 randomly sampled subsets of the PDX data obtained by removing 10 samples from the PDX data (the ones used in training in a few-shot setting) and keeping the remaining ones as a test set. Of note, the number of test samples depends on the perturbation, as all treatments are not measured in all PDX.

Machine learning framework

We aim to predict perturbation response (gene dependency or drug response) based on gene expression data. Some of our models additionally use perturbation-specific fingerprints as input.

Overall modeling approach

To predict perturbation response, we use a regression algorithm which takes a lower dimensional representation of the data as input. We compare two types of regression approaches: a perturbation-specific approach based on multiple models (PS) where independent regressors are trained to predict the response for each perturbation, and a pan-perturbation model approach (PP) where we predict the response to any (perturbation, disease model) pair based on the gene expression of the disease model and the fingerprints of the perturbation. Our approach can be decomposed into three steps where we (i) train a Data-Augmented Masked Auto Encoder (DAMAE) to represent the RNAseq data, (ii) extract the first 500 components from a Principal Component Analysis (PCA) of the fingerprint data (for the pan-perturbation model approach only), and (iii) train a regression algorithm using the data embeddings as input¹². Under the perturbation-specific (PS) paradigm, we consider baseline K-nearest neighbors (PS-KNN), LASSO regressors (PS-LASSO), and LightGBM models (PS-LGBM), each trained on a single perturbation's data. We also include TCRP¹¹ and three pan-perturbation (PP) methods: PP-LGBM and tDNN, with the latter further adapted into PP-MLP. For a fair comparison of the regression approaches, all methods are integrated with our DAMAE in place of their original autoencoders (we study the added value of the DAMAE compared to a regular AE in figure 1). To improve the prediction performance of all models (except for the baseline PS-KNN), we use ensembling by aggregating the predictions obtained with multiple regressors trained on different subsets of the data. In LEAP, we further ensemble multiple PS-LASSO models trained on different data representations obtained with different initializations (Figure 1).

Representation algorithm

We train representation learning models on RNAseq data to generate embeddings for the disease models (cell lines or PDX). These representation models are agnostic to the perturbation as they only depend on the molecular profiles of the disease models. The

OmicsRPZ¹² study demonstrated superior performance in predicting gene dependency by employing a Masked Auto-Encoder (MAE) or a Gaussian Noise Data Augmented Auto-Encoder (DA-GN). Building on this foundation, we combined the two best performing methods into a method referred to as Data Augmented Masked Auto-Encoder (DAMAE), for RNAseq representation.

Inspired by regularization techniques⁴⁸, we combined a masking technique with the addition of Gaussian noise to each batch of the Auto-Encoder. For masking, we started from the method developed in VIME⁴⁹ and we adapted it to (i) remove the mask-predict pretext-task, which didn't improve the prediction performance of the downstream task but also significantly increased training time (results not shown), and (ii) optimize the mask allocation code. For each training batch, we randomly mask 30% of the input entries in the batch data matrix and use the VIME corruption method to permute these masked entries with values coming from other samples. Additionally, we apply data augmentation by adding a small Gaussian noise (std=0.01) to every batch. We fix the representation dimensionality and several other parameters of the MAE based on the settings used in the OmicsRPZ paper. The representation dimension is fixed at 256, with 512 units in the first hidden layer, a dropout rate of 0.2, and training capped at 3000 epochs with early stopping (patience=20, delta=10⁻⁵).

Since we are in a transductive task setup, and to reduce computational burden, we do not train distinct DAMAE models on the different training sets used for each of the 5 tasks. Instead, we train the DAMAE model only once using all available unlabelled samples with RNAseq measurements across the DepMap⁵, PharmacDB²⁷ and PDX Encyclopedia²⁸ datasets, totalling 1920 cell lines and 191 PDX. The same DAMAE model is then used for all tasks (Figure 1). We investigate the impact of this choice in an ablation study and show that surprisingly this does not improve performances (Supplementary Figure 4). In LEAP, we propose to use an ensemble of 5 DAMAE models obtained with different random seeds to leverage variability in this procedure and eventually increase robustness and prediction performance²⁰. The change in random seed affects the selection of the early stopping holdout set, the dropout, masking, and augmentation operations, and the initialization of the different layers. The 4 additional DAMAE models are trained on the same dataset including all unlabelled samples.

For the pan-perturbation approach, we also use representation models trained on the gene or drug fingerprints. As in the OmicsRPZ study, we utilized Principal Component Analysis (PCA) to reduce the dimensionality of the fingerprint data.

Regression algorithms

We consider seven modeling approaches. For a fair comparison across the prediction models approach, we used them jointly with our DAMAE and considered limited grids of up to 10 combinations of parameters. In methods that incorporate already an AE, we replace their AE with our DAMAE.

The perturbation-specific K nearest neighbor⁵⁰ (**PS-KNN**) constitutes a baseline in our study. In PS-KNN, the response to a given perturbation is predicted as the average response observed

for the K nearest cell lines based on their gene expression profile which have available response to the perturbation of interest. We considered the K=5 nearest neighbors.

In **PS-LASSO**, we train one LASSO⁵¹ model for each perturbation. Each of the regressors in PS-LASSO takes molecular features (RNAseq) of the cell lines as input. The hyper-parameters of each of the regressors in PS-LASSO are tuned independently by maximizing prediction performance for the corresponding perturbation. We considered a small grid of 10 automatically defined values of the L1-regularization parameter using the sklearn library.

Similarly, we train one LGBM for each perturbation in **PS-LGBM**. This LGBM has 400 estimators with a maximum depth of 10 and 31 leaves. We tuned the learning rate and the proportion of features to keep in each subsample. We considered a limited grid of two values for the learning rate (0.005 and 0.01) and five values for the feature proportion (0.05, 0.1, 0.15, 0.2 or 0.25).

Next, we include **PS-TCRP**¹¹, a perturbation-specific method leveraging model-agnostic meta-learning to predict perturbation response from cell line data. This approach was originally proposed with pre-training in cell lines and fine-tuning in (i) an unseen tissue, (ii) patient-derived cell lines, or (iii) patient-derived xenografts. More recently, it was fine-tuned in patients¹⁵. We use 2 layers of 20 neurons each, which constitute the largest structure tested in the original paper. As recommended, we use 200 epochs and 12 inner learning tasks corresponding to 12 randomly sampled tissues at each epoch. We considered a limited grid of two values for the meta-learning rates (0.0005, 0.001) and five values for the inner-learning rate (0.0005, 0.001, 0.002, 0.005, 0.01). For the out-of-domain tasks (tasks 3, 4, and 5), we report performances of both zero-shot TCRP, where the model is trained with meta-learning but no fine-tuning, and 10-shot TCRP to assess the benefit of incorporating a small number of target samples.

In **PP-LGBM**, we use a pan-perturbation regression model to predict the response to any perturbation in a given cell line based on both sample-level features (RNAseq) and perturbation-level features (fingerprints)^{10,12}. As in the OmicsRPZ study¹², we use an LGBM with 500 estimators, a maximum depth of 20 and 4,000 leaves, and we tuned the learning rate and the L1-regularization parameter. We considered a limited grid of five values for the learning rate (0.01, 0.02, 0.03, 0.04 and 0.05) and two values for the regularization parameter (0 or 1).

We also incorporate **PP-tDNN**¹⁸, a pan-perturbation deep neural network model designed to integrate gene expression and drug fingerprints through two subnetworks. Each subnetwork has three dense hidden layers, whose outputs are concatenated and passed through four additional hidden layers with consecutive halvings of nodes. Dropout layers follow all but the last hidden layer. Initial parameters and architecture are as defined in previous work¹⁸. We use a grid of five values for the dropout rate (0, 0.1, 0.25, 0.45, 0.7).

Finally, we introduce **PP-MLP**, a version of tDNN tuned to enhance performance in our study. Unlike the original tDNN, PP-MLP employs tailored hyperparameter settings and additional regularization to improve predictive accuracy across perturbations.

Hyper-parameter tuning procedure

We use grid search to tune the hyper-parameters of all regression models, except the baseline PS-KNN. For each combination of hyper-parameters, we perform a 5-fold cross-validation within the training data, maximizing the per-perturbation Spearman's correlation.

For PS approaches, we tune the hyper-parameters of each perturbation-specific regression model separately. For PP approaches, we tune the hyper-parameters of the pan-perturbation regression model by maximizing the average per-perturbation Spearman's correlation.

For challenges I and III, we use 5 folds made of non-overlapping sets of cell lines. For challenge II, we use one tissue per fold in order to improve the generalisability of the model for predictions in an unseen tissue.

Layered ensembling

To improve prediction performances in LEAP, we use an ensemble model where the final prediction is defined as the average of the predictions obtained from multiple regressors. For this, we first use the 5 DAMAE models to generate 5 different representations of the training data. The regressors trained in each iteration of the cross-validation conducted on each of the 5 representations of the data are used for ensembling. A total of 25 regressors are ensembled, coming from the data embeddings of 5 DAMAE models and for each, 5 regressors trained in a 5-fold CV.

Performance metrics

Prediction performance is measured by comparing the true and predicted perturbation response in the test set of unseen cell lines (challenge I), cell lines from an unseen tissue (challenge II), or unseen PDX (challenge III).

As in previous work, we use the Spearman's and Pearson's correlations as performance metrics¹². We report both (i) the average of per-perturbation correlations measured by comparing the true and predicted responses to each of the perturbations and (ii) the overall correlation measured by comparing the true and predicted response for all sample-perturbation pairs in the test set.

Contributions

- Conceptualization and Research Direction: AD, BB, GD
- Methodology and Evaluation Design: AD, BB, GD
- Software Development and Review: BB, GD, AD
- Formal Analysis – Model Development (Representation and Ensembling): AD, GD
- Formal Analysis – Model Development (Prediction Models, Tuning): BB, GD, AD

- Investigation and Experiments: BB, GD, AD
- Visualizations: GD, BB, LB
- Writing: BB, AD, GD, LB
- Supervision and Coordination: AD

Declaration of Competing Interest

All authors are employees of Owkin, Inc., New York, NY, USA.

Acknowledgements

We wanted to thank Eric Durand, Jean-Philippe Vert, Floriane Montanari, Mathieu Andreux, John Klein and Geneviève Robin for their scientific guidance and feedback on the manuscript. We thank Roberta Cortado and Rita Santos for their recommendations on the choice of experimental labels. We thank Chiara Regniez for her related work on transfer learning tasks. We are also grateful to contributors involved in earlier phases of the project: Jean El Khoury contributed to the initial data augmentation development and ensembling tests, Khalil Ouardini implemented the initial masking, Quentin Klopfenstein and Hugo Malafosse assisted with testing and tuning initial perturbation-specific models.

References

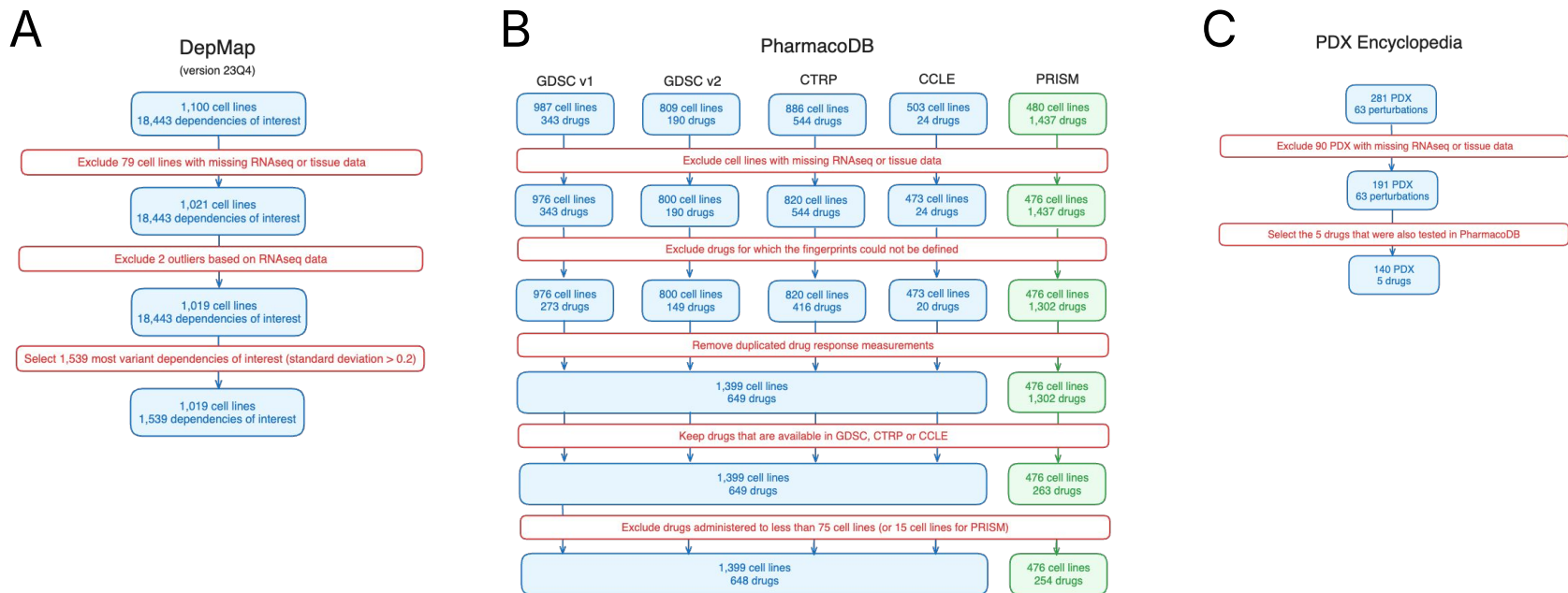
1. Kim, H. S., Sung, Y.-J. & Paik, S. Cancer Cell Line Panels Empower Genomics-Based Discovery of Precision Cancer Medicine. *Yonsei Med. J.* **56**, 1186 (2015).
2. Wildey, M. J., Haunso, A., Tudor, M., Webb, M. & Connick, J. H. High-Throughput Screening. in *Annual Reports in Medicinal Chemistry* vol. 50 149–195 (Elsevier, 2017).
3. Ibarrola-Villava, M., Cervantes, A. & Bardelli, A. Preclinical models for precision oncology. *Biochim. Biophys. Acta BBA - Rev. Cancer* **1870**, 239–246 (2018).
4. Mezencev, R. & Subramaniam, R. The use of evidence from high-throughput screening and transcriptomic data in human health risk assessments. *Toxicol. Appl. Pharmacol.* **380**, 114706 (2019).
5. Tsherniak, A. *et al.* Defining a Cancer Dependency Map. *Cell* **170**, 564–576.e16 (2017).
6. Yang, W. *et al.* Genomics of Drug Sensitivity in Cancer (GDSC): a resource for therapeutic biomarker discovery in cancer cells. *Nucleic Acids Res.* **41**, D955–D961 (2012).
7. Barretina, J. *et al.* The Cancer Cell Line Encyclopedia enables predictive modelling of anticancer drug sensitivity. *Nature* **483**, 603–607 (2012).
8. Basu, A. *et al.* An Interactive Resource to Identify Cancer Genetic and Lineage Dependencies Targeted by Small Molecules. *Cell* **154**, 1151–1161 (2013).
9. Corsello, S. M. *et al.* Discovering the anticancer potential of non-oncology drugs by systematic viability profiling. *Nat. Cancer* **1**, 235–248 (2020).
10. Chiu, Y.-C. *et al.* Predicting and characterizing a cancer dependency map of tumors with deep learning. *Sci. Adv.* **7**, eabh1275 (2021).
11. Ma, J. *et al.* Few-shot learning creates predictive models of drug response that translate from high-throughput screens to individual patients. *Nat. Cancer* **2**, 233–244 (2021).
12. Gross, B. *et al.* Robust evaluation of deep learning-based representation methods for survival and gene essentiality prediction on bulk RNA-seq data. *Sci. Rep.* **14**, 17064 (2024).
13. Ding, M. Q., Chen, L., Cooper, G. F., Young, J. D. & Lu, X. Precision Oncology beyond

- Targeted Therapy: Combining Omics Data with Machine Learning Matches the Majority of Cancer Cells to Effective Therapeutics. *Mol. Cancer Res.* **16**, 269–278 (2018).
14. Sharifi-Noghabi, H., Harjandi, P. A., Zolotareva, O., Collins, C. C. & Ester, M. Out-of-distribution generalization from labelled and unlabelled gene expression data for drug response prediction. *Nat. Mach. Intell.* **3**, 962–972 (2021).
 15. He, D., Liu, Q., Wu, Y. & Xie, L. A context-aware deconfounding autoencoder for robust prediction of personalized clinical drug response from cell-line compound screening. *Nat. Mach. Intell.* **4**, 879–892 (2022).
 16. Preuer, K. *et al.* DeepSynergy: predicting anti-cancer drug synergy with Deep Learning. *Bioinformatics* **34**, 1538–1546 (2018).
 17. Kuenzi, B. M. *et al.* Predicting Drug Response and Synergy Using a Deep Learning Model of Human Cancer Cells. *Cancer Cell* **38**, 672-684.e6 (2020).
 18. Zhu, Y. *et al.* Ensemble transfer learning for the prediction of anti-cancer drug response. *Sci. Rep.* **10**, 18040 (2020).
 19. Ahlmann-Eltze, C., Huber, W. & Anders, S. Deep learning-based predictions of gene perturbation effects do not yet outperform simple linear methods. Preprint at <https://doi.org/10.1101/2024.09.16.613342> (2024).
 20. Fort, S., Hu, H. & Lakshminarayanan, B. Deep Ensembles: A Loss Landscape Perspective. *arXiv.org* <https://arxiv.org/abs/1912.02757v2> (2019).
 21. Abe, T., Buchanan, E. K., Pleiss, G., Zemel, R. & Cunningham, J. P. Deep Ensembles Work, But Are They Necessary? in *Advances in Neural Information Processing Systems* (eds. Koyejo, S. *et al.*) vol. 35 33646–33660 (Curran Associates, Inc., 2022).
 22. Lakshminarayanan, B., Pritzel, A. & Blundell, C. Simple and Scalable Predictive Uncertainty Estimation using Deep Ensembles. in *Advances in Neural Information Processing Systems* (eds. Guyon, I. *et al.*) vol. 30 (Curran Associates, Inc., 2017).
 23. Haghverdi, L., Lun, A. T. L., Morgan, M. D. & Marioni, J. C. Batch effects in single-cell RNA

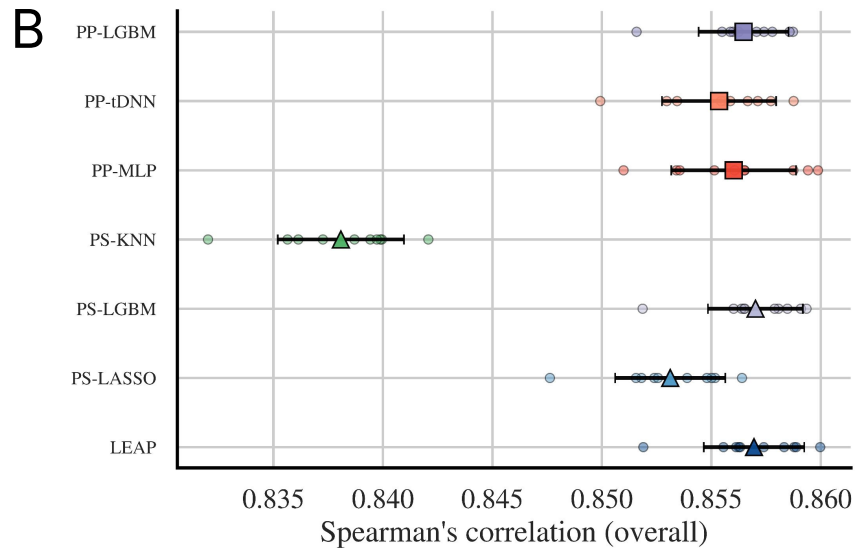
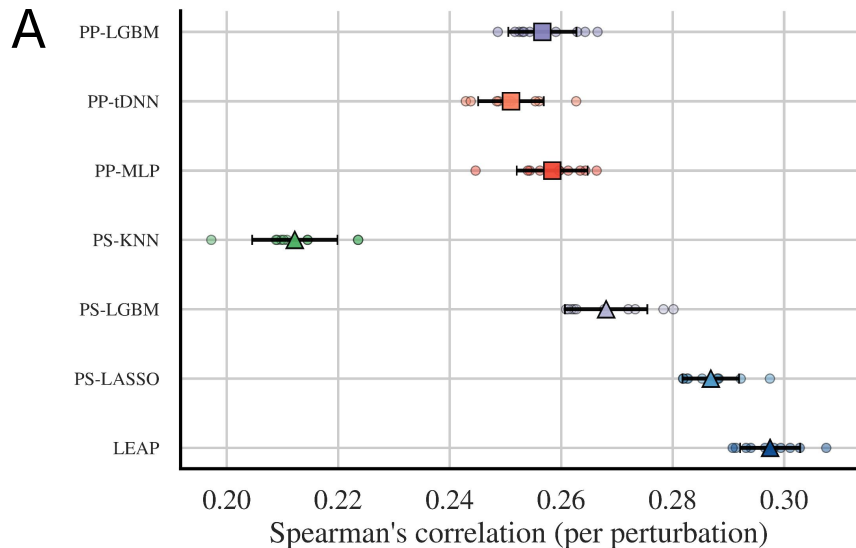
- sequencing data are corrected by matching mutual nearest neighbours. *Nat. Biotechnol.* **36**, 421–427 (2018).
24. Warren, A. *et al.* Global computational alignment of tumor and cell line transcriptional profiles. *Nat. Commun.* **12**, 22 (2021).
 25. Zhang, Y., Parmigiani, G. & Johnson, W. E. ComBat-seq: batch effect adjustment for RNA-seq count data. *NAR Genomics Bioinforma.* **2**, lqaa078 (2020).
 26. Korsunsky, I. *et al.* Fast, sensitive and accurate integration of single-cell data with Harmony. *Nat. Methods* **16**, 1289–1296 (2019).
 27. Smirnov, P. *et al.* PharmacoDB: an integrative database for mining in vitro anticancer drug screening studies. *Nucleic Acids Res.* **46**, D994–D1002 (2018).
 28. Gao, H. *et al.* High-throughput screening using patient-derived tumor xenografts to predict clinical trial drug response. *Nat. Med.* **21**, 1318–1325 (2015).
 29. Meyers, R. M. *et al.* Computational correction of copy number effect improves specificity of CRISPR–Cas9 essentiality screens in cancer cells. *Nat. Genet.* **49**, 1779–1784 (2017).
 30. Pozdeyev, N. *et al.* Integrating heterogeneous drug sensitivity data from cancer pharmacogenomic studies. *Oncotarget* **7**, 51619–51625 (2016).
 31. Geeleher, P., Gamazon, E. R., Seoighe, C., Cox, N. J. & Huang, R. S. Consistency in large pharmacogenomic studies. *Nature* **540**, E1–E2 (2016).
 32. So, E., Yu, F., Wang, B. & Haibe-Kains, B. Reusability report: Evaluating reproducibility and reusability of a fine-tuned model to predict drug response in cancer patient samples. *Nat. Mach. Intell.* **5**, 792–798 (2023).
 33. Ovchinnikova, K., Born, J., Chouvardas, P., Rapsomaniki, M. & Kruithof-de Julio, M. Overcoming limitations in current measures of drug response may enable AI-driven precision oncology. *Npj Precis. Oncol.* **8**, 95 (2024).
 34. Cho, Y.-H. Review on Advanced Cancer Modeling for a Cancer Study. *Curr. Issues Mol. Biol.* **44**, 5352–5362 (2022).

35. Dempster, J. M. *et al.* Extracting Biological Insights from the Project Achilles Genome-Scale CRISPR Screens in Cancer Cell Lines. 720243 Preprint at <https://doi.org/10.1101/720243> (2019).
36. Pacini, C. *et al.* Integrated cross-study datasets of genetic dependencies in cancer. *Nat. Commun.* **12**, 1661 (2021).
37. Dempster, J. M. *et al.* Chronos: a cell population dynamics model of CRISPR experiments that improves inference of gene fitness effects. *Genome Biol.* **22**, 343 (2021).
38. Ghandi, M. *et al.* Next-generation characterization of the Cancer Cell Line Encyclopedia. *Nature* **569**, 503–508 (2019).
39. DepMap 22Q4 Public. figshare <https://doi.org/10.6084/m9.figshare.21637199.v2> (2022).
40. Smirnov, P. *et al.* PharmacoGx: an R package for analysis of large pharmacogenomic datasets. *Bioinformatics* **32**, 1244–1246 (2016).
41. Iorio, F. *et al.* A Landscape of Pharmacogenomic Interactions in Cancer. *Cell* **166**, 740–754 (2016).
42. Gur, C. *et al.* LGR5 expressing skin fibroblasts define a major cellular hub perturbed in scleroderma. *Cell* **185**, 1373-1388.e20 (2022).
43. Liberzon, A. *et al.* Molecular signatures database (MSigDB) 3.0. *Bioinforma. Oxf. Engl.* **27**, 1739–1740 (2011).
44. Kim, S., Thiessen, P. A., Cheng, T., Yu, B. & Bolton, E. E. An update on PUG-REST: RESTful interface for programmatic access to PubChem. *Nucleic Acids Res.* **46**, W563–W570 (2018).
45. Winter, R., Montanari, F., Noé, F. & Clevert, D.-A. Learning continuous and data-driven molecular descriptors by translating equivalent chemical representations. *Chem. Sci.* **10**, 1692–1701 (2019).
46. RDKit: Open-source cheminformatics.
47. Sharifi-Noghabi, H. *et al.* Drug sensitivity prediction from cell line-based pharmacogenomics

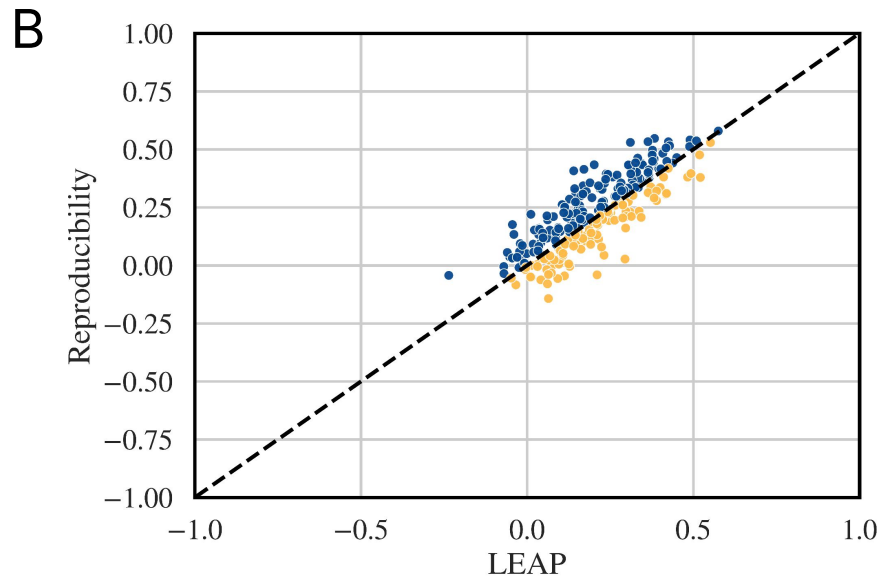
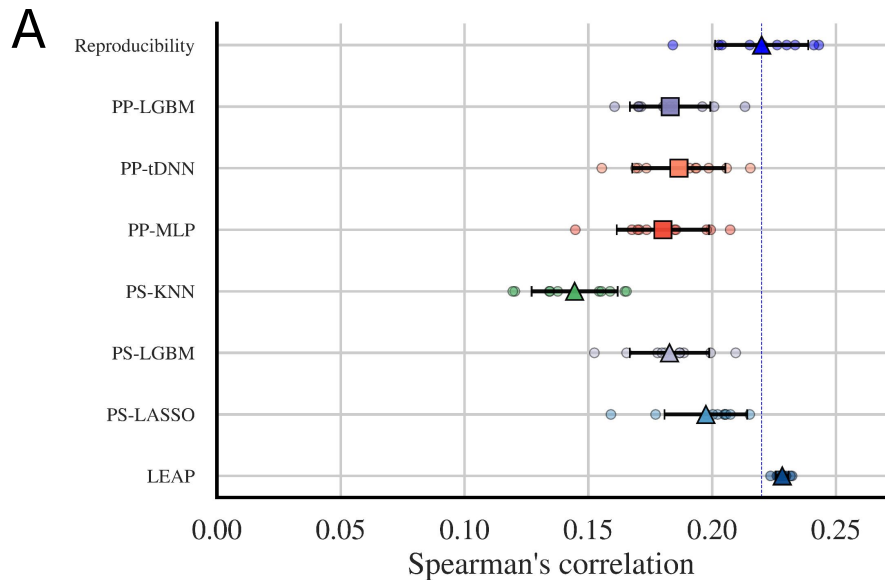
- data: guidelines for developing machine learning models. *Brief. Bioinform.* **22**, bbab294 (2021).
48. Adam, G. *et al.* Machine learning approaches to drug response prediction: challenges and recent progress. *Npj Precis. Oncol.* **4**, 19 (2020).
49. Yoon, J., Zhang, Y., Jordon, J. & van der Schaar, M. VIME: Extending the Success of Self- and Semi-supervised Learning to Tabular Domain. in *Advances in Neural Information Processing Systems* (eds. Larochelle, H., Ranzato, M., Hadsell, R., Balcan, M. F. & Lin, H.) vol. 33 11033–11043 (Curran Associates, Inc., 2020).
50. Guo, G., Wang, H., Bell, D., Bi, Y. & Greer, K. KNN Model-Based Approach in Classification. in *On The Move to Meaningful Internet Systems 2003: CoopIS, DOA, and ODBASE* (eds. Meersman, R., Tari, Z. & Schmidt, D. C.) vol. 2888 986–996 (Springer Berlin Heidelberg, Berlin, Heidelberg, 2003).
51. Tibshirani, R. Regression Shrinkage and Selection Via the Lasso. *J. R. Stat. Soc. Ser. B Stat. Methodol.* **58**, 267–288 (1996).



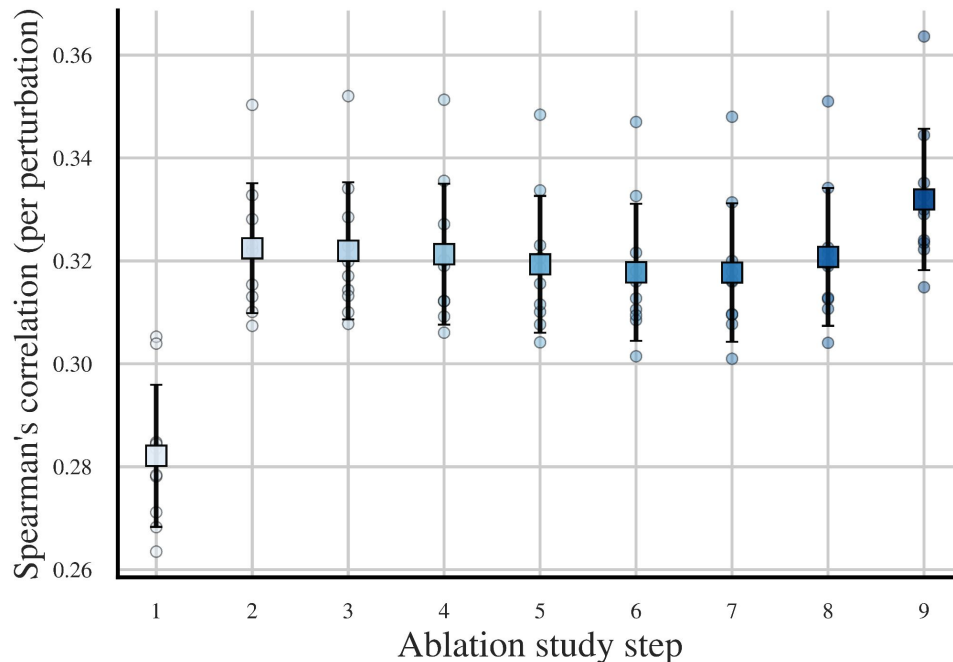
Supplementary Figure 1. Flowcharts illustrating the data preparation steps. We report each step of our procedure to select cell lines and perturbations in DepMap (A), PharmacDB (B) and PDX Encyclopedia (C).



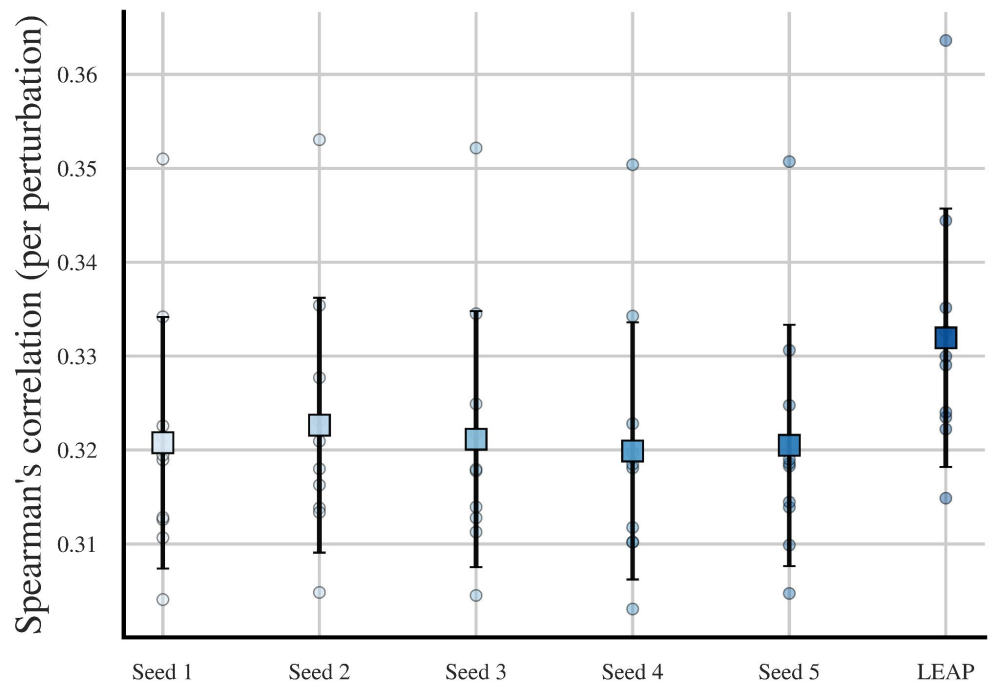
Supplementary Figure 2. Comparison of the performances in predicting gene dependency in unseen cell lines (task 1b) using different models. We compare the performance of our novel approach (LEAP, in blue) with other models. Performances are evaluated over 10 splits of the data. For each data split, we report the average Spearman's correlation between observed and predicted gene dependencies for each of the 1,223 dependencies of interest (A), or the overall Spearman's correlation between observed and predicted gene dependency over all pairs of genes and cell lines (B). The distribution of correlation coefficients obtained over the 10 training-test splits is represented as a boxplot. Each point indicates the correlation obtained in one of the 10 training-test splits.



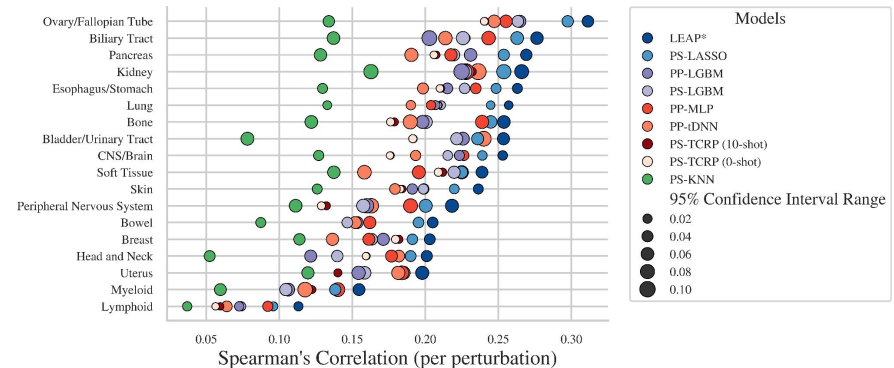
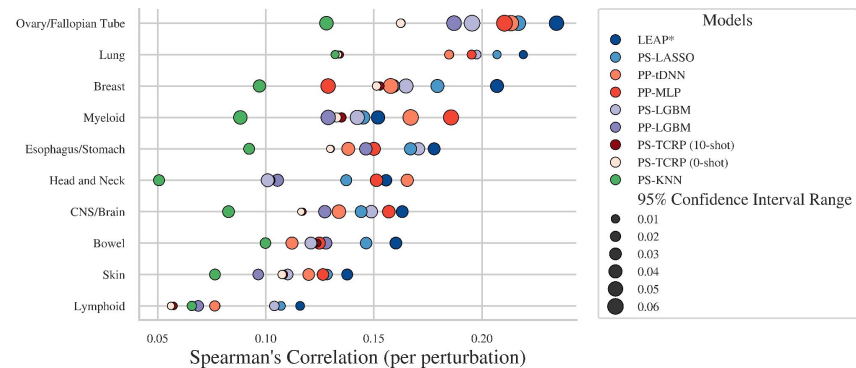
Supplementary Figure 3. Comparison of prediction performances with drug response reproducibility across studies. For each drug, label reproducibility is quantified by the Spearman's correlation in response to 257 drugs measured in the same 468 cell lines in the training studies (GDSC, CTRP and CCLE) and the external validation study (PRISM). We report the average Spearman's correlation across all drugs available in both the training and validation studies. Prediction performances are evaluated in the same cell lines and drugs for all the approaches that were trained in task 2a. To ensure models are tested on unseen cell line-drug pairs, we repeat this procedure 10 times, each time excluding the training pairs from PRISM. This results in 10 distinct test sets. (A). We also compare LEAP performances with label reproducibility for each of the 257 drugs (B).



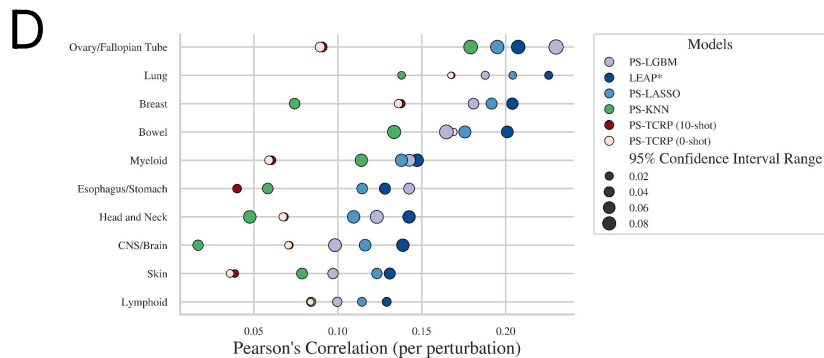
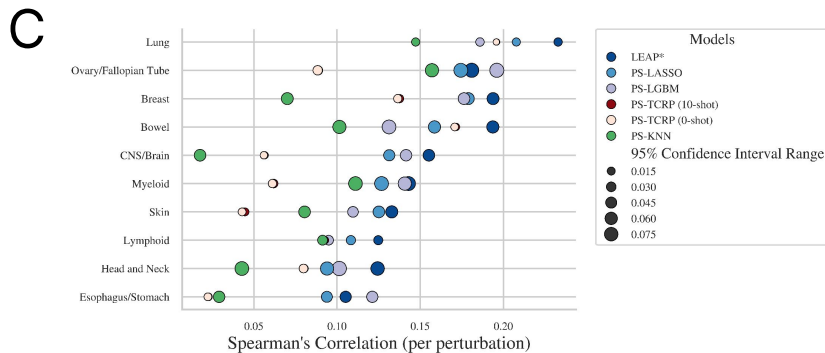
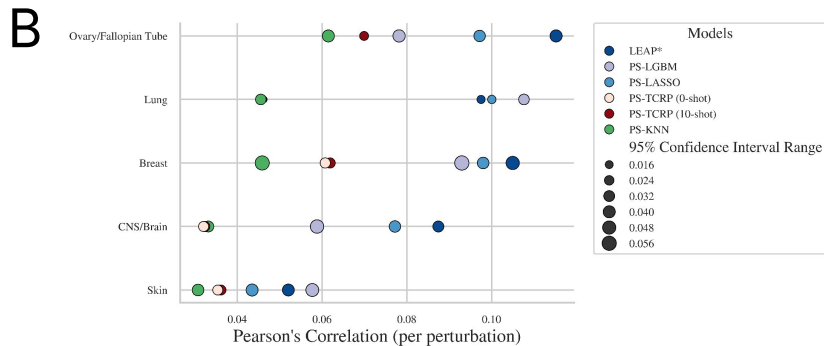
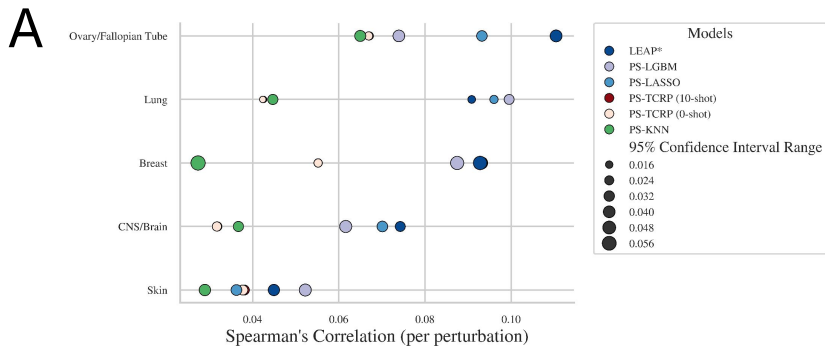
Supplementary Figure 4. Change in prediction performances in task 1a due to each of the methodological choices. In step 1, we use the state-of-the-art approach implemented in OmicsRPZ (REF). In step 2, we use multiple LASSO regression models instead of a single LGBM model. In step 3, we use the gene expression data of 7,083 genes instead of 5,000 genes. In step 4, we standardize the data using the mean and standard deviation calculated on the full DepMap dataset. In step 5, we also train the DAMAE on the full DepMap dataset. We then train the preprocessing and DAMAE using data from DepMap and GDSC (step 6), or DepMap, GDSC and PDXE (step 7). In step 8, we ensemble the 5 regression models trained in the 5-fold CV. In step 9, we ensemble 25 regression models that were trained in the 5-fold CV and using 5 DAMAE models obtained with different random seeds. This ablation study is further described in Supplementary Table 4



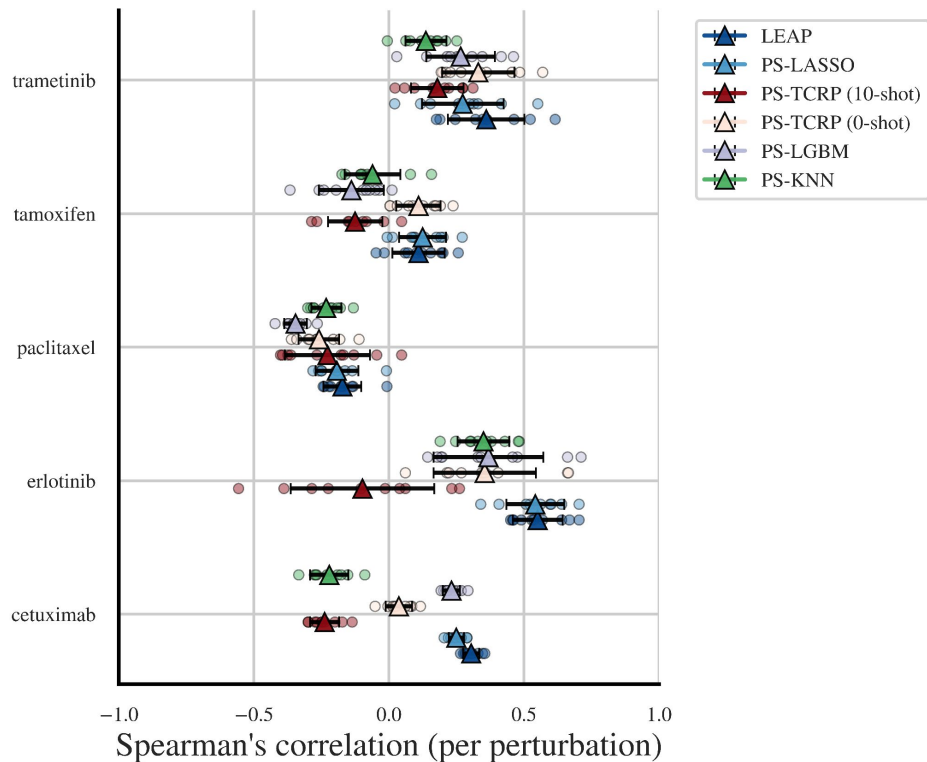
Supplementary Figure 5. Prediction performances obtained with PS-LASSO using each of the 5 seeds or with LEAP in task 1a. We report the performances obtained with each of the 5 PS-LASSO models using different DAMAE models. Prediction performance is measured by the Spearman's correlation between observed and predicted gene dependencies in task 1a.

**A****B**

Supplementary Figure 6. Performance in predicting perturbation response by tissue (tasks 3a and 4a). We evaluate the performances in predicting gene dependency (A, task 3a) or drug response (B, task 4a) in cell lines from an unseen tissue. For each tissue, we report the median Spearman's correlation between observed and predicted responses per perturbation, after 1000 interactions of bootstrapping. The size of each data point is proportional to the range of the 95% confidence interval of the corresponding perturbation-specific correlations.



Supplementary Figure 7. Performances of POWSER in predicting perturbation response in unseen tissues using former versions of the data for comparability (tasks 3b and 4b). We evaluate the performances in predicting gene dependency (A and B, task 3b) or drug response (C and D, task 4b) in cell lines from an unseen tissue. For each tissue, we report the median Spearman's (A and C) or Pearson's (B and D) correlation between observed and predicted responses per perturbation, after 1000 interactions of bootstrapping. The size of each data point is proportional to the range of the 95% confidence interval of the corresponding perturbation-specific correlations.



Supplementary Figure 8. Performances in predicting the response to 5 drugs in PDX samples (task 5a). To assess variability and be as comparable as possible to published results, we report the mean (standard deviation) of these metrics calculated over 10 subsets of the data obtained by removing 10 PDX samples.

Supplementary Table 1. Overview of the available data for model training and evaluation (after data preparation).

Study	Sub-study	Disease model	Label	RNAseq data acquired	Number of tissues	Number of samples	Number of perturbations	Number of sample x perturbation pairs	Dosages (drug response only)
DepMap	23Q4	Cell line	Gene dependency	Yes	27	1,019	1,539	1,568,222	-
	22Q4		Gene dependency	Yes	27	893	1,223	1,092,139	-
	18 (first release)		Gene effect	from 23Q4	20	335	469	156,646	-
Pharmacodb	GDSC v1	Cell line	Area Above the drug dose-response Curve (AAC)	Yes	28	976	343	284,823	
	GDSC v2			Yes	26	800	176	127,053	
	CTRP			No	25	820	544	346,032	
	CCLC			No	23	473	24	10,757	
	PRISM			No	21	476	254	644,437	
PDX Encyclopedia		Patient-derived xenograft		Yes	4	140	5	227	-

Note: 20 tissues in 1b and not 19 as in Fewshot as:

- HAEMATOPOIETIC_AND_LYMPHOID_TISSUE is split between Lymphoid and Myeloid
- OESOPHAGUS and STOMACH are merged in Esophagus/Stomach
- SF767_CENTRAL_NERVOUS_SYSTEM is "Cervix" in latest metadata for its OncotreeLineage (and not CNS as others)

Note 2:

- 335 CLs in DepMap in Fewshot.
- In the labels downloaded, 342 cell lines and by removing the ones without RNAseq AND mutations (needed for fewshot) there are 337 cell lines.
- 2 of the 337 are not in most recent CCLC so are dropped too, total of 335 for us too

Supplementary Table 2. Performances in predicting gene dependency in unseen cell lines (task 1b). We compare the performance of our novel approach (LEAP) with a baseline model (M-KNN), a state-of-the-art model (S-LGBM) and previously reported performances obtained using different representation models in OmicsRPZ (REF). Performances are evaluated over 10 splits of the data into non-overlapping sets of cell lines. For each data split, we report the average Spearman's correlation between observed and predicted gene dependencies calculated over all 1,223 dependencies of interest. For each training-test split, we calculate the mean perturbation-specific Spearman's correlations, Pearson's correlations and Mean Squared Errors comparing observed and predicted gene dependencies. We report the mean (standard deviation) of these metrics calculated over the 10 training-test splits. Note that the performances of OmicsRPZ model were not recomputed and were obtained with different training-test splits of the same dataset.

Approach	Spearman's correlation
OmicsRPZ (Identity)	0.2369 (0.0058)
OmicsRPZ (PCA)	0.2461 (0.0055)
OmicsRPZ (AE)	0.2489 (0.0078)
OmicsRPZ (scVI)	0.2452 (0.0139)
OmicsRPZ (MHAE)	0.2489 (0.0032)
OmicsRPZ (MAE)	0.2551 (0.0059)
OmicsRPZ (DA-GN)	0.2559 (0.0059)
OmicsRPZ (GNN)	0.2502 (0.0095)
M-KNN	0.2122 (0.0076)
S-LGBM	0.2566 (0.0061)
LEAP	0.2975 (0.0054)

Supplementary Table 3. Performances in predicting perturbation response in unseen cell lines, unseen tissue or unseen disease model. We compare the performance of our novel approach (LEAP) with a baseline model (M-KNN) and a state-of-the-art model (S-LGBM). We evaluate the performances in predicting gene dependency in unseen cell lines (task 1a), drug response in unseen cell lines (task 2a), drug response in unseen cell lines from the external validation dataset (task 2a PRISM), gene dependency in an unseen tissue (task 3a), drug response in an unseen tissue (task 4a), and drug response in PDX (task 5a). Performances are evaluated over 10 splits of the data into non-overlapping training and test sets for tasks 1a, 2a and 5a, or by sequentially using each tissue as a test set for tasks 3a and 4a. For each data split, we calculate the average Spearman's correlations, Pearson's correlations and Mean Squared Error comparing observed and predicted responses per perturbation. We report the mean (standard deviation) of these metrics calculated over the training-test splits. We do not report the Mean Squared Error for task 5a as the metrics are on different scales.

Task	Model	Per-perturbation			Overall		
		Spearman's correlation	Pearson's correlation	Mean Squared Error	Spearman's correlation	Pearson's correlation	Mean Squared Error
1a	PP-LGBM	0.2844 (0.0177)	0.3005 (0.0188)	0.0657 (0.0008)	0.6508 (0.0061)	0.6539 (0.0055)	0.0657 (0.0008)
	PP-tDNN	0.286 (0.0158)	0.3002 (0.0173)	0.0668 (0.0007)	0.6497 (0.0063)	0.6514 (0.0059)	0.0668 (0.0007)
	PP-MLP	0.3048 (0.0134)	0.3184 (0.015)	2.2297 (0.8018)	0.6539 (0.0063)	0.6553 (0.0061)	2.2297 (0.8018)
	PS-KNN	0.2278 (0.0096)	0.2416 (0.0099)	0.0745 (0.001)	0.6048 (0.005)	0.6083 (0.0049)	0.0745 (0.001)
	PS-LGBM	0.3028 (0.0144)	0.3177 (0.0151)	0.0653 (0.0007)	0.6539 (0.0047)	0.6569 (0.0043)	0.0653 (0.0007)
	PS-LASSO	0.3208 (0.0134)	0.3335 (0.0139)	0.0654 (0.0008)	0.656 (0.0057)	0.6575 (0.0051)	0.0654 (0.0008)
	LEAP	0.3319 (0.0138)	0.3447 (0.0142)	0.0642 (0.0008)	0.6627 (0.0055)	0.6647 (0.0049)	0.0642 (0.0008)
2a	PP-LGBM	0.3351 (0.015)	0.3685 (0.0103)	0.0088 (0.0003)	0.7547 (0.0049)	0.8089 (0.0036)	0.0099 (0.0003)
	PP-tDNN	0.3302 (0.0138)	0.3629 (0.0096)	0.0088 (0.0003)	0.756 (0.0046)	0.8132 (0.0037)	0.0098 (0.0003)
	PP-MLP	0.3409 (0.0148)	0.3695 (0.0114)	369595.4454 (338535.7906)	0.7567 (0.005)	0.8126 (0.0044)	397843.1691 (364238.4092)
	PS-KNN	0.298 (0.014)	0.3261 (0.0096)	0.0098 (0.0003)	0.7308 (0.0055)	0.7886 (0.005)	0.011 (0.0004)
	PS-LGBM	0.3349 (0.0153)	0.3673 (0.0104)	0.0088 (0.0003)	0.7537 (0.0053)	0.8082 (0.0039)	0.0099 (0.0003)
	PS-LASSO	0.3387 (0.0119)	0.3692 (0.01)	0.0089 (0.0003)	0.7449 (0.006)	0.8082 (0.0042)	0.01 (0.0003)
	LEAP	0.3504 (0.0119)	0.3809 (0.0101)	0.0087 (0.0003)	0.752 (0.0056)	0.813 (0.0039)	0.0097 (0.0003)
3a	PP-LGBM	0.1905 (0.0532)	0.2022 (0.0558)	0.0676 (0.0046)	0.6392 (0.0199)	0.6428 (0.0207)	0.0676 (0.0046)
	PP-tDNN	0.1851 (0.0498)	0.1936 (0.0548)	0.0701 (0.007)	0.631 (0.0336)	0.6332 (0.0344)	0.0701 (0.007)
	PP-MLP	0.2046 (0.0462)	0.2135 (0.0488)	2.5837 (0.8651)	0.6375 (0.0289)	0.6394 (0.0298)	2.5837 (0.8651)
	PS-KNN	0.1142 (0.043)	0.1199 (0.0449)	0.0784 (0.0047)	0.5811 (0.0184)	0.5857 (0.0194)	0.0784 (0.0047)
	PS-LGBM	0.1916 (0.0509)	0.2026 (0.0536)	0.0679 (0.005)	0.6372 (0.022)	0.6409 (0.023)	0.0679 (0.005)
	PS-LASSO	0.2192 (0.0476)	0.2289 (0.0494)	0.0698 (0.0095)	0.6341 (0.0335)	0.6332 (0.0408)	0.0698 (0.0095)
	LEAP	0.233 (0.0469)	0.243 (0.0481)	0.0674 (0.0071)	0.6443 (0.0288)	0.6458 (0.0318)	0.0674 (0.0071)
4a	PP-LGBM	0.1303 (0.039)	0.1443 (0.0481)	0.0108 (0.0035)	0.7288 (0.0275)	0.7711 (0.0154)	0.0118 (0.0038)
	PP-tDNN	0.1446 (0.0401)	0.1588 (0.0481)	0.011 (0.004)	0.7199 (0.0264)	0.7667 (0.0218)	0.012 (0.0044)
	PP-MLP	0.1474 (0.0411)	0.1605 (0.0496)	182.0222 (387.6747)	0.7233 (0.03)	0.7663 (0.0224)	192.2368 (415.4878)
	PS-KNN	0.0896 (0.0267)	0.0986 (0.0306)	0.0119 (0.0033)	0.6975 (0.0313)	0.7436 (0.0224)	0.0131 (0.0036)
	PS-LGBM	0.1424 (0.0374)	0.1582 (0.048)	0.0108 (0.0036)	0.7327 (0.0282)	0.7747 (0.0174)	0.0118 (0.0038)
	PS-LASSO	0.1558 (0.0362)	0.1667 (0.0436)	0.0112 (0.0042)	0.7195 (0.0275)	0.764 (0.0231)	0.0123 (0.0046)
	LEAP	0.1695 (0.039)	0.1794 (0.0467)	0.0107 (0.0035)	0.7276 (0.0271)	0.7743 (0.0157)	0.0117 (0.0039)

Supplementary Table 4. Ablation study quantifying the change in prediction performance due to each of the methodological choices. We start from the state-of-the-art approach implemented in OmicsRPZ (REF) where (i) the data is standardised, (ii) an AMAE is trained, and (iii) a single LGBM model is trained on the AMAE-transformed data to predict gene dependency (step 1). In step 2, we change the regression strategy to use one Elastic Net regression per perturbation instead of the single LGBM. In step 3, we increase the number of input genes by concatenating most variant genes identified in DepMap, GDSC and PDXE. In step 4, we standardise the data based on the means and standard deviations calculated in the full DepMap data and not only in the training set. In step 5, the AMAE is also trained in the full DepMap data instead of the training set only. In steps 6 and 7, we sequentially add the GDSC and PDXE data to train the preprocessor and AMAE. In step 8, we ensemble the 5 regression models trained in the different cross-validation splits. Finally, in step 9, we further ensemble the 5 sets of models obtained from 5 AMAE models trained using different random seeds. For each of the 10 training-test splits used in task 1a, we calculate the mean perturbation-specific Spearman's correlations between observed and predicted gene dependencies. We report the mean (standard deviation) of this metric calculated over the 10 training-test splits.

Ablation study step	Number of input genes	Dataset for preprocessing model training	Dataset for representation model training	Regression model	Number of representation models for ensembling	Total number of prediction models for ensembling	Spearman's correlation
1	5,000	Training set	Training set	LGBM	1	1	0.2821 (0.0138)
2	5,000	Training set	Training set	Elastic net	1	1	0.3224 (0.0126)
3	7,083	Training set	Training set	Elastic net	1	1	0.322 (0.0133)
4	7,083	Full DepMap (version 23Q4)	Training set	Elastic net	1	1	0.3213 (0.0137)
5	7,083	Full DepMap (version 23Q4)	Full DepMap (version 23Q4)	Elastic net	1	1	0.3193 (0.0133)
6	7,083	Full DepMap (version 23Q4) and GDSC	Full DepMap (version 23Q4) and GDSC	Elastic net	1	1	0.3178 (0.0133)
7	7,083	Full DepMap (version 23Q4), GDSC and PDX Encyclopedia	Full DepMap (version 23Q4), GDSC and PDX Encyclopedia	Elastic net	1	1	0.3177 (0.0134)
8	7,083	Full DepMap (OmicsRPZ), GDSC and PDX Encyclopedia	Full DepMap (OmicsRPZ), GDSC and PDX Encyclopedia	Elastic net	1	5	0.3208 (0.0134)
9	7,083	Full DepMap (OmicsRPZ), GDSC and PDX Encyclopedia	Full DepMap (OmicsRPZ), GDSC and PDX Encyclopedia	Elastic net	5	25	0.3319 (0.0138)

Supplementary Table 5. Performances in predicting gene essentiality in unseen cell lines using different ensembling strategies (task 1a). We compare the prediction performances in task 1a using LEAP or using M-ENET with ensembling fo 25 regression models obtained over 5 repeats of 5-fold cross-validation. Performances are evaluated over 10 splits of the data into non-overlapping training and test sets. For each training-test split, we calculate the average Spearman's correlations, Pearson's correlations and Mean Squared Error comparing observed and predicted responses per perturbation. We report the mean (standard deviation) of these metrics calculated over the training-test splits.

Approach	Spearman's correlation	Pearson's correlation	Mean Squared Error
M-ENET (ensemble of 5 models)	0.3208 (0.0134)		
M-ENET (ensemble of 25 models)	0.3221 (0.0136)	0.335 (0.0141)	0.0652 (0.0008)
LEAP	0.3319 (0.0138)	0.3447 (0.0142)	0.0642 (0.0008)

Supplementary Table 6. Performances in predicting perturbation response in unseen tissue using LEAP with different cross-validation strategies. We compare the prediction performances in tasks 3a and 4a using LEAP with hyper-parameter tuning based on (i) 5-fold cross-validation with a split by cell line, (ii) grouped 5-fold cross-validation ensuring that different tissues are distributed over the 5 folds, and (iii) leave-one-tissue-out cross-validation. Performances are evaluated by sequentially using each tissue as a test set for tasks 3a and 4a. For each out-of-domain tissue, we calculate the average Spearman's correlations, Pearson's correlations and Mean Squared Error comparing observed and predicted responses per perturbation. We report the mean (standard deviation) of these metrics calculated over the training-test splits.

Task	Approach	Spearman's correlation	Pearson's correlation	Mean Squared Error
3a	5-fold CV	0.2333 (0.0475)	0.2433 (0.049)	0.0678 (0.0073)
	Grouped 5-fold CV by tissue	0.233 (0.0469)	0.243 (0.0481)	0.0674 (0.0071)
	Leave-one-tissue-out CV	0.2314 (0.0476)	0.2412 (0.0494)	0.0688 (0.0088)
4a	5-fold CV	0.1645 (0.0422)	0.1749 (0.0496)	0.0118 (0.0053)
	Grouped 5-fold CV by tissue	0.1695 (0.039)	0.1794 (0.0467)	0.0107 (0.0035)
	Leave-one-tissue-out CV	0.1627 (0.0402)	0.1719 (0.0468)	0.0112 (0.0042)

Supplementary Table 7. Performances in predicting the response to 5 drugs in PDX samples (task 5b). For comparability with published results (REF), we train our novel approach (LEAP) to predict the AUC in cell lines from the GDSC study. We evaluate performances in PDX using the Spearman's and Pearson's correlations between predicted and observed response to each of the drugs. To assess variability and be as comparable as possible to published results, we report the mean (standard deviation) of these metrics calculated over 10 subsets of the data obtained by removing 10 PDX samples.

Drug	Spearman's correlation	Pearson's correlation
Cetuximab	0.2490 (0.0316)	0.3596 (0.0266)
Erlotinib	0.5589 (0.0323)	0.6069 (0.0203)
Tamoxifen	0.0368 (0.0793)	-0.0710 (0.0752)
Trametinib	0.2705 (0.0633)	0.4393 (0.0758)
Paclitaxel	-0.2757 (0.0158)	-0.3568 (0.0136)